Final Technical Report
USGS Award G14AP00034

Evaluation of the Southern California Seismic Velocity Models Through Ground Motion Simulation and Validation of Past Earthquakes

Ricardo Taborda,[1,2,*] Shima Azizzadeh-Roodpish,[1,2]
Naeem Khoshnevis,[2] and Keli Cheng[3]

[1] Department of Civil Engineering, The University of Memphis, TN 38152
[2] Center for Earthquake Research and Information, The University of Memphis, Memphis TN 38152
[3] Department of Computer Science, The University of Memphis, Memphis TN 38152
[*] Corresponding author, e-mail: ricardo.taborda@memphis.edu

PI: Ricardo Taborda
Start Date: April 1, 2014
End Date: June 30, 2015
Department of Civil Engineering, and
Center for Earthquake Research and Information
The University of Memphis
Memphis, TN 38152

Report Summary

Current efforts in forward seismic wave propagation simulation of earthquakes, full waveform tomography, physics-based probabilistic seismic hazard analysis, earthquake forecasting and early warning systems are intrinsically dependent on the accuracy and availability of seismic source and velocity models. With the exception of inverse problems, in most cases, these models are de-facto accepted input parameters. The existing models are, however, far from perfect. Previous validation efforts conducted by the PI showed that even for moderate-magnitude earthquakes, where the influence of the source model is less relevant and the presence of nonlinear and topographic site effects can be omitted, significant deviation exists between synthetic results and recorded data. Such efforts also indicated that the accuracy of the velocity models used for simulation was an important factor in the quality of the fit. Prior to this project, the PI and his collaborators have also shown that for the case of southern California in particular, the various velocity models available could lead to significantly different results, even at low frequencies ($f \leq 0.5$ Hz). These initial efforts, however, were conducted for a single historical event.

The main goal of this project was therefore to perform a similar comparative validation study of the seismic velocity models available for the region of Southern California using simulations and recorded time-series, but extending this effort to a larger number of events. We used physics-based, deterministic simulations to reproduce the ground motion of a set of 30 earthquakes ($3.6 < M < 5.4$). Each earthquake was simulated using the various velocity models available for the region, namely CVM-S4, CVM-S4.26, and CVM-H (with and without its GTL module). All simulations were done in a common fixed simulation domain. The simulation synthetics were compared with records from strong motion and broadband stations, and validated using a quantitative goodness-of-fit criterion. Through the validation process, in which the level of agreement between simulations and data was quantified systematically across velocity models and events, we sought to identify which of the velocity models consistently leads to better simulation results, and thus make recommendations for future simulations.

The following report summarizes the work done under the project plan and presents the current state of additional analysis and interpretation being done (beyond those tasks considered within the project's framework). As a guide to the reader, it should be noted that this report is also the initial version of a manuscript in preparation to be submitted to the *Geophysical Journal International.* This project directly supported a full time Ph.D. student in the Geophysics program of the Center for Earthquake Research and Information at the University of Memphis, and provided indirect support and research opportunities for a Ph.D. student in Civil Engineering and an undergraduate student in Computer Science, also at the University of Memphis. These students are co-authors of this report and associated publications derived from this research project.

Publications resulted from this project

Azizzadeh-Roodpish, S., Khoshnevis, N., and Taborda, R. (2014). Evaluation of the southern california velocity models through simulation and validation of multiple historical events. In *Proc. SCEC Annu. Meet.*, number CME 080, Palm Springs, CA, September 6–10.

Azizzadeh-Roodpish, S., Taborda, R., Khoshnevis, N., and Cheng, K. (2015). Evaluation of the scec seismic velocity models through simulation and validation of past earthquakes. In *Proc. SCEC Annu. Meet.*, number CME 037, Palm Springs, CA, September 12–16.

Taborda, R., Azizzadeh-Roodpish, S., Khoshnevis, N., and Cheng, K. (2016). Evaluation of the southern California seismic velocity models through simulation and validation of historical events. *Geophys. J. Int.* Manuscript in preparation (to be submitted October 2015).

Evaluation of the Southern California Seismic Velocity Models Through Ground Motion Simulation and Validation of Past Earthquakes

Ricardo Taborda,[1,2,*] Shima Azizzadeh-Roodpish,[1,2]
Naeem Khoshnevis,[2] and Keli Cheng[3]

[1] Department of Civil Engineering, The University of Memphis, TN 38152
[2] Center for Earthquake Research and Information, The University of Memphis, Memphis TN 38152
[3] Department of Computer Science, The University of Memphis, Memphis TN 38152
[*] Corresponding author, e-mail: ricardo.taborda@memphis.edu

1 Introduction

There exist a good number of seismic velocity models developed for different regions around the world such as southern and northern California in the United States (Kohler et al., 2003; Brocher et al., 2006); the Grenoble and Volvi valleys in Europe (Chaljub et al., 2010; Manakou et al., 2010); and Japan (Koketsu et al., 2008; Fujiwara et al., 2009). While some of these and other models of smaller regions have been built for specific research activities (e.g. Graves, 2008; Maufroy et al., 2015), the last two decades have seen an increasing interest for developing models that can be applied more broadly, and that can be continuously updated by a community of users. These models are known as community velocity models, or CVMs. The United States Geological Survey (USGS), for instance, recently released two such models, the Wasatch Front Community Velocity Model (WFCVM) for the region of the Salt Lake basin and the Wasatch fault (Magistrale et al., 2006), and the Central United States Velocity Model (CUSVM) for the region of the New Madrid seismic zone (Ramírez-Guzmán et al., 2012).

Among the various velocity models available in the U.S., the models developed and maintained by the Southern California Earthquake Center (SCEC), CVM-S and CVM-H, stand out as good examples of community models. These CVMs have evolved over time with contributions from a community of researchers who share an interest in studying the earthquake hazards and ground motion characteristics in southern California. CVM-S, also known as CVM-S4, was originally developed by Magistrale et al. (1996) and later updated by Magistrale et al. (2000) and Kohler et al. (2003). Recently, a new version of CVM-S, called CVM-S4.26 was built based on the original model and the results of a sequence of 3D full-waveform tomographic inversions done by Chen et al. (2007) and Lee et al. (2014b). CVM-H, on the other hand, was originally developed by Süss and Shaw (2003) and then periodically improved by Plesch et al. (2007, 2008, 2009, 2011). Some of the later additions to CVM-H include results from inversions done by Tape et al. (2009, 2010) and the inclusion of an optional geotechnical layer (GTL) model based on Ely et al. (2010).

Both the CVM-S and CVM-H families of models are regarded as acceptable representations of the crustal structure in southern California, at least at low frequencies ($f \leq 0.2$ Hz). Nonetheless, it is known that they have distinctions that can lead to significantly different results, even at these very low frequencies (e.g. Lee et al., 2014a; Taborda and Bielak, 2014). Such differences, however, have never been systematically evaluated in forward simulations, or at frequencies beyond the upper limits set by the underlying inversions used to construct the models. Taborda and Bielak (2014), for instance, showed that simulations for the 2008 M_w 5.4 Chino Hills, California, earthquake using the models CVM-S and CVM-H exhibited meaningful differences in the results. They used a goodness-of-fit (GOF) criteria to compare synthetics to data and concluded that the choice of the velocity model had a significant effect on the outcome of the simulations, concluding that, at least for the particular case of Chino Hills, CVM-S4 led to better fits than CVM-H, especially at frequencies below 1 Hz. In turn, Lee et al. (2014a) compared results obtained using CVM-S4, CVM-S4.26 and CVM-H for simulations of the 2014 M_w 5.1 La Habra and 2014 M_w 4.4 Encino earthquakes. In both cases, the authors showed that CVM-S4.26 led to better fits between 0.02 and 0.2 Hz.

In this project we evaluated the southern California velocity models when used to predict the ground motion in the greater Los Angeles basin and its surrounding areas. The evaluation was carried out by means of validation of multiple simulations, through quantitative comparisons between synthetics and data, for a collection historical events. In total, we considered 30 earthquakes and used four different seismic velocity models: CVM-S4, CVM-S4.26, and CVM-H with the GTL option active and inactive. We refer to CVM-H with the GTL option active as CVM-H+GTL. All the earthquakes were of moderate size, with moment magnitudes (M_w) between 3.5 and 5.5, and occurred between 1998 and 2014, with epicenters spread throughout a simulation domain with a surface projection area of 180 km × 135 km. The simulations were performed using a finite element application for solving forward wave propagation problems under kinematic faulting (Tu et al., 2006; Taborda et al., 2010), with a numerical model built to represent a maximum frequency, $f_{\max} = 1$ Hz and a minimum shear wave velocity, $V_{S_{\min}} = 200$ m/s.

We based our evaluation of the different simulations on the GOF scores obtained following a modified version of the criteria introduced by Anderson (2004). Our results indicate that the simulations done with the model CVM-S4.26 consistently yield better fits with data than the synthetics obtained with CVM-S4, CVM-H and CVM-H+GTL. This indicates that previous observations made by Taborda and Bielak (2014) and Lee et al. (2014a) where not exclusive to the cases considered by these authors. More important, it indicates that the improvements done to CVM-S based on the tomographic studies done by Chen et al. (2007) and Lee et al. (2014a) have positive effects at frequencies above the limit considered for the inversions (0.2 Hz).

2 Region of Interest and Velocity Models

We considered a region of interest covering the entire Los Angeles metropolitan area and most of the significant geologic structures in its vicinity. This includes the greater Los Angeles, Chino, and San Bernardino basins; the San Fernando and Simi valleys; the San Gabriel, Santa Ana, and Santa Monica mountains; and part of the Mojave desert, the Santa Clara river valley, and the Ventura basin in a simulation domain of size 180 km × 135 km × 62 km (Fig. 1).

The elastic properties within the simulation domain are determined based on the models CVM-S4, CVM-S4.26, CVM-H, and CVM-H+GTL. At any given query point, each of these models provides the values of the P- and S-wave velocities (V_P and V_S), and the material's density (ρ). CVM-S4 was initially developed by Magistrale et al. (1996), and later improved by Magistrale et al. (2000) and Kohler et al. (2003). In particular, we use version 4, release 11.11.0. This model integrates available information about the major southern California basins using data from boreholes, oil-well samples, gravity observations, and seismic refraction surveys. The model in itself is built upon empirical rules that use the depths and ages estimated for a set of geological horizons calibrated for southern California. Below and outside the basins, CVM-S4 relies on the 3D seismic tomography model proposed by Hauksson (2000), and an upper-mantle model based on teleseismic inversions introduced into the model by Kohler et al. (2003).

The second model, CVM-S4.26, is a model recently developed by SCEC based on the results from a full 3D tomography (F3DT) inversion done by Lee et al. (2014b). The inversion process involved a sequence of 26 iterations over a reference model extracted from CVM-S4, thus its name. This effort followed the procedure first applied to the Los Angeles region by Chen et al. (2007). In Lee et al. (2014b), the reference model corresponded to a regular grid of 500-m spacing in which the material properties extracted from CVM-S4 were truncated to minimum values of $V_P = 2000$ m/s, $V_S = 1000$ m/s and $\rho = 2000$ kg/m^3. The truncation was smoothed until the values extracted from the model reached 3000 m/s, 2000 m/s and 2300 kg/m^3, respectively. To compute the perturbations to the initial model, Lee et al. (2014b) used about 38,000 earthquake records and 12,000 ambient noise Green's functions, and combined two inversion methods, the adjoint-wavefield method (AW-F3DT; Tromp et al., 2005) and the scattering-integral method (SI-F3DT; Zhao et al., 2006). Each iteration in the procedure involved the computation of a forward simulation done using a staggered-grid finite-differences approach (Olsen, 1994). The forward simulations

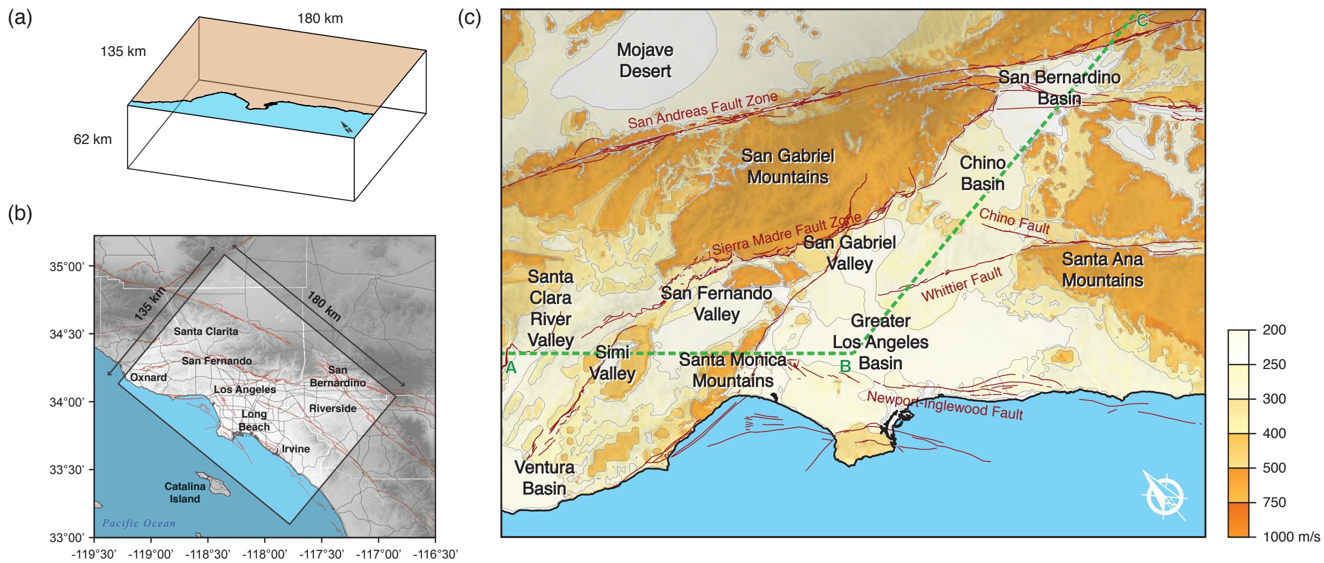

Figure 1: Region of interest and simulation domain. (a) 3D view of the simulation domain. (b) Geographical location and surface projection of the simulation domain, along with the names of the main cities surrounding the Los Angeles metropolitan are. (c) Major geologic structures including basins, valleys and mountains, along with the main quaternary faults in the region. The color background represents the surface V_{S30} values included in the CVM-H+GTL model, with a topography shading effect. The segments $\overline{\text{AB}}$ and $\overline{\text{BC}}$ are used as reference for Fig. 3.

were done for a maximum frequency, $f_{\max} = 0.2$ Hz; and the misfits were computed using seismograms band-pass filtered at 0.02–0.2 Hz. After the 26th iteration perturbations were obtained, the results were merged with the original CVM-S4 model using an interpolation scheme to recover the truncated values. The result is the CVM-S4.26 model.

In turn, CVM-H was originally developed by Süss and Shaw (2003) and has since undergone multiple periodic updates (Plesch et al., 2007, 2008, 2009, 2011). Similarly to CVM-S4, CVM-H is built using the regional seismic travel-time tomography model of Hauksson (2000) in the background, but with differences in the structure of the basins. The major basins in CVM-H were defined using seismic reflection profiles and tens of thousands of borehole measurements (Süss and Shaw, 2003). A particular aspect of CVM-H is that its structural representation is compatible with the geometry of major faults in southern California, as represented in the SCEC Community Fault Model (Plesch et al., 2007; Shaw et al., 2015). Besides the background tomography, the model also incorporates information from upper-mantle teleseismic and surface-wave models extending to depths of 300 km (Prindle and Tanimoto, 2006); and as done in the case of CVM-S4.26, CVM-H was improved using results from an AW-F3DT inversion process with 16 iterations (Tape et al., 2009, 2010). Here, we use CVM-H version 11.9.1. Although there is a more recent version (15.1.0), the changes in the latter pertain to structures out of the simulation domain. CVM-H also includes a GTL model. We, however, refer to CVM-H alone as the model with the GTL option inactive.

Last, we use the model CVM-H+GTL, which is the same as CVM-H but with the GTL option active. This model incorporates an algorithm proposed by Ely et al. (2010) to soften the material properties in the near-surface layers. The procedure uses the characteristic value of V_S in the top 30 m (V_{S30}) in order to modify the free-surface V_S and then interpolate the values of V_S, V_P and ρ with depth, until they match those of the original model at depth, $z = 350$ m. The values of V_{S30} are obtained from a geology-based map developed by Wills and Clahan (2006) for California, and the slope-dependent (topography-based) estimation proposed by Wald and Allen (2007) for points outside California. By default, the GTL model is active in CVM-H as distributed by SCEC. However, for evaluation purposes, we refer to it as if it were a different model (CVM-H+GTL). This is especially relevant

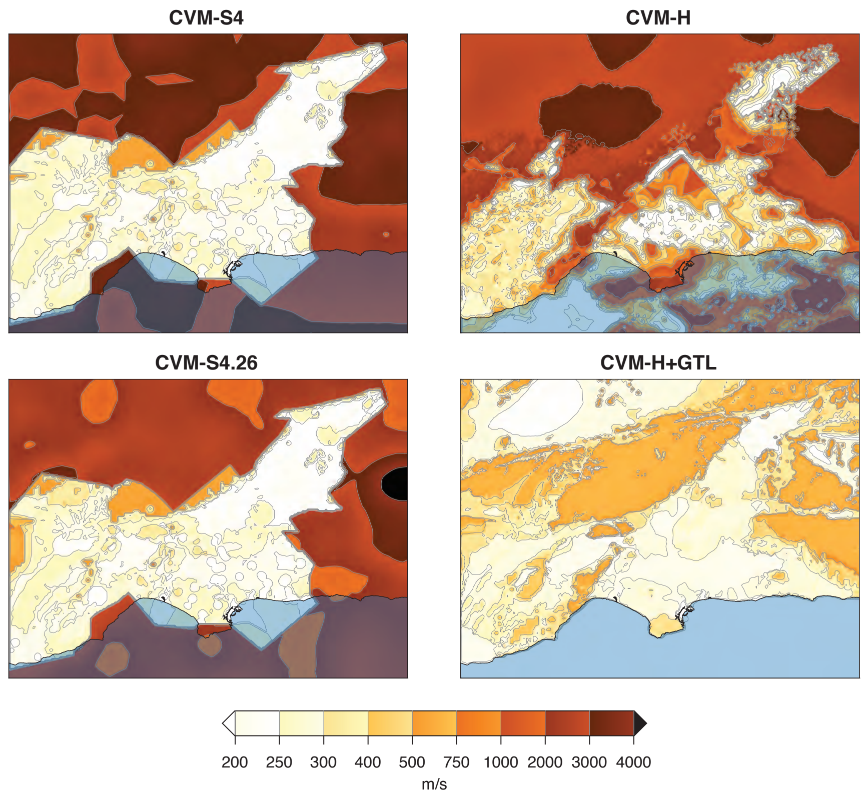

Figure 2: Comparison between the southern California community velocity models considered as seen in the free-surface shear wave velocity (V_S) of each model.

because previous related work suggests that the approach used to implement the GTL model in CVM-H introduces changes in the shape of the basins and their velocity contrasts with the bedrock (Taborda and Bielak, 2014).

In all cases, we constructed rasterized versions of the models using the Unified Community Velocity Model (UCVM) software framework developed by SCEC (Small et al., 2011; Gill et al., 2015), and the UCVM implementation of the etree library (Tu et al., 2003), which follows a similar procedure to that described in Taborda et al. (2007) and Schlosser et al. (2008).

Fig. 2 shows a comparison between the four models for the free-surface V_S. Although the models have some general similarities, especially within each of the two families, the images in the figure clearly illustrate some of the more relevant contrasts. From the isosurfaces, for instance, it is seen that CVM-S4 and CVM-S4.26 are as similar near the surface ($z < 1$ km), as CVM-H and CVM-H+GTL are similar at depth ($z > 0.5$ km). This is consistent, on the one hand, with the construction of CVM-S4.26 as this model was derived from a F3DT that had $V_{S_{\min}} = 1000$ m/s. Meaning that the changes near the surface are the result of the interpolation done when merging the inversion perturbations with the reference model, and not a direct consequence of the F3DT. On the other hand, we do not expect to see any difference between CVM-H and CVM-H+GTL beyond $z = 350$ m, as this is the depth at which the interpolation done when activating the GTL model matches the values of the original CVM-H model. Perhaps the larger contrasts between CVM-S4 and CVM-S4.26 are observed off shore and north of the San Andreas fault, in the Mojave desert (see Fig. 1 for reference). Other changes are observable in the Santa Clara river valley and Ventura basin, and in the vicinity of the San Bernardino basin, especially to the East (top-right corner of the simulation domain). In all these cases CVM-S4.26 exhibits deeper structures than CVM-S4.

The strongest contrast between the CVM-H and CVM-H+GTL models with respect to CVM-S4 and CVM-S4.26 is in the San Fernando, Santa Clara river and Simi valleys, and the Ventura basin. Here, the structure in CVM-H is deeper and wider than in CVM-S4 and CVM-S4.26. Between CVM-H and CVM-H+GTL, the most relevant

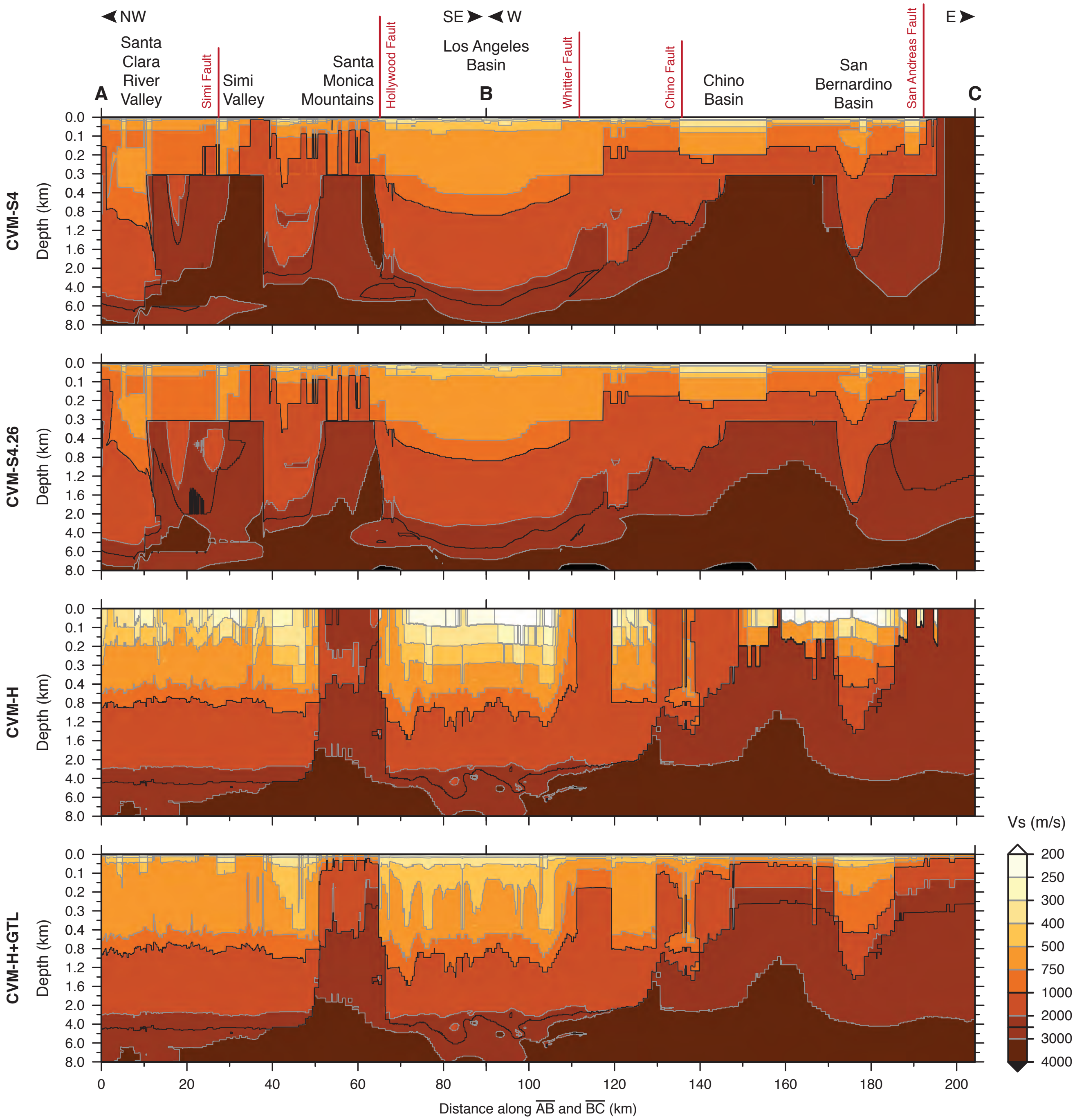

Figure 3: Vertical profiles of shear wave velocity (V_S) along the segments $\overline{\mathrm{AB}}$ and $\overline{\mathrm{BC}}$ shown in Fig. 1 for each of the models considered. Markers and labels at the top indicate crossings of the profiles through significant geologic structures and seismic faults. The vertical scales of the profiles are unevenly exaggerated in three segments from 0 to 0.4 km, 0.4 to 2 km, and 2 to 8 km to highlight the differences between the models, especially near the surface.

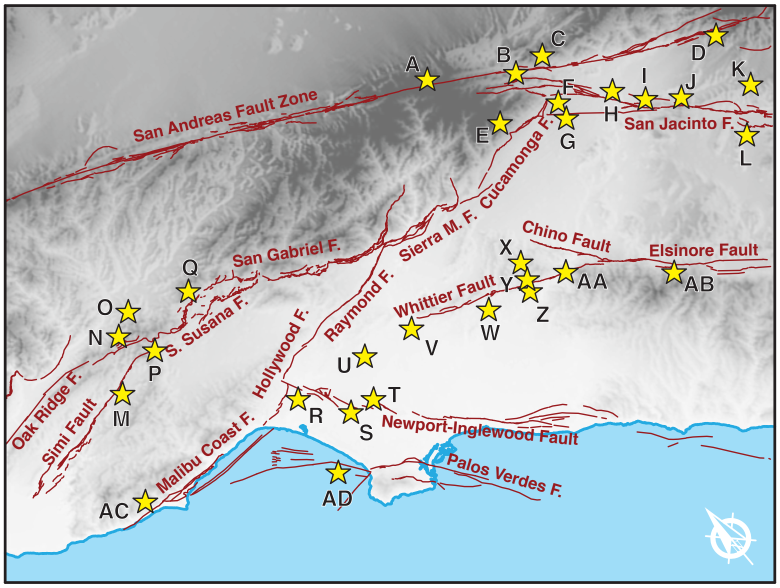

Figure 4: Location of the epicenters within the simulation domain for the 30 events considered here, along with some of the major quaternary faults in the region. The events are labeled with a sequential letter-code. Details about the magnitude, date and focal mechanism are provided in Table 1.

changes are along the edges of the basins and, in particular, in the shape and depth of the San Bernardino basin. These differences between the models are seen more clearly in Fig. 3, where we compare two contiguous vertical profiles (V_S) along the segments $\overline{\mathrm{AB}}$ and $\overline{\mathrm{BC}}$ shown in Fig. 1. Note that most of the changes in CVM-S4.26 with respect to CVM-S4 are in the deeper structures, and to the north-west of the of segment $\overline{\mathrm{AB}}$ and to the east of segment $\overline{\mathrm{BS}}$. This figure also highlights the effects of the GTL model in CVM-H+GTL with respect to CVM-H, with the most relevant changes in the western section of the San Bernardino basin, the softer profiles introduced between the Chino basin and the Whittier fault, as well as the beneath the Santa Monica mountains, and the reduction of the thickness of the deposits.

3 Selected Earthquakes

We considered 30 earthquakes in the region within the simulation domain. The selected events, scattered throughout, occurred between 1998 and 2014, and had magnitudes between 3.6 and 5.4, and hypocenter depths that vary between 3.6 and 21.1 km. The largest events considered are the 2008 M_w 5.4 Chino Hills earthquake, followed by the 2014 M_w 5.1 La Habra earthquake, which are the strongest earthquakes registered in the region since the 1994 M_w 6.7 Northridge earthquake. Fig. 4 shows the location of the epicenters, which we labeled with a sequential letter-code from A to Z, and AA to AD. Also shown in the figure are the main seismic faults in the region. Table 1 provides detailed information about each of the selected events, including the event's ID, magnitude, hypocenter coordinates and depth, focal mechanism (strike, dip, and rake angles), and date and time (in coordinated universal time, or UTC). The coordinates, depth, and focal mechanisms correspond to those obtained by Lee et al. (2011) using a full-wave centroid moment tensor inversion.

We modeled each event considering a point source analogy with rupture parameters scaled according to the magnitude of each earthquake. First, we computed the rupture dimensions using the general expressions proposed by Wells and Coppersmith (1994) for all types of faults to obtain the subsurface rupture length (l_s) and downdip rupture width (w_d). Then, following the analogy of a circular fault area, and assuming that in the vicinity of a

Table 1: Selected events and description of source location, magnitude, focal mechanism,

Code	Earthquake name	Event ID	M_w	Coordinates (lon., lat.)	Depth (m)	Strike/Dip/Rake	Date (yyyy/mm/dd)	UTC Time (hh:mm:ss)	Num. Stns.
A	Wrightwood	9064568	4.40	–117.6480, 34.3740	8.99	285/57/86	1998/08/20	23:49:58.198	17
B	NW of Devore	10972299	3.79	–117.4642, 34.2655	10.91	98/58/68	2001/07/19	20:42:36.470	52
C	NNE of Devore	14494128	3.72	–117.3838, 34.2587	7.18	344/69/-33	2009/08/01	12:55:55.317	82
D	Yucaipa	14155260	4.88	–117.0113, 34.0580	11.61	75/59/55	2005/06/16	20:53:26.225	173
E	N of Rancho Cucamonga	10216101	3.60	–117.5762, 34.2058	4.92	54/69/16	2006/11/04	19:43:44.376	56
F	2002 Fontana	13692644	3.74	–117.4288, 34.1613	6.54	233/72/-28	2002/07/25	00:43:14.872	55
G	2005 Fontana	14116972	4.42	–117.4387, 34.1250	4.15	222/88/-25	2005/01/06	14:35:27.593	83
H	San Bernardino	10370141	4.45	–117.3042, 34.1073	14.22	87/70/28	2009/01/09	03:49:46.051	163
I	N of Loma Linda	9140050	4.37	–117.2525, 34.0500	15.36	270/90/-6	2000/02/21	13:49:43.017	38
J	Redlands	10541957	4.10	–117.1797, 34.0045	8.53	33/46/-68	2010/02/13	21:39:06.349	103
K	2010 Beaumont	10530013	4.28	–117.0232, 33.9322	13.93	234/89/9	2010/01/16	12:03:25.345	82
L	2006 Beaumont	14239184	3.90	–117.1122, 33.8560	11.53	45/31/-25	2006/07/10	02:54:43.809	65
M	Simi Valley	14000376	3.59	–118.7530, 34.2722	13.81	234/62/60	2003/10/29	23:44:48.206	54
N	WSW of Valencia	9753489	3.90	–118.6678, 34.3705	14.21	83/62/57	2002/01/29	06:00:39.140	52
O	N of Pico Canyon	9096972	3.98	–118.6090, 34.3980	11.53	287/55/54	1999/07/22	09:57:23.502	26
P	Chatsworth	14312160	4.66	–118.6195, 34.2995	7.58	82/27/51	2007/08/09	07:58:48.888	113
Q	Newhall	15237281	3.86	–118.4580, 34.3508	3.59	236/58/33	2012/10/28	15:24:23.172	128
R	Beverly Hills	9703873	4.24	–118.3885, 34.0590	7.90	262/81/4	2001/09/09	23:59:17.695	130
S	Inglewood Area	10410337	4.70	–118.3357, 33.9377	13.86	243/60/25	2009/05/18	03:39:36.126	219
T	NW of Compton	9716853	3.98	–118.2702, 33.9290	21.13	116/68/71	2001/10/28	16:27:45.388	55
U	Downtown Los Angeles	9093975	3.77	–118.2180, 34.0100	9.53	125/49/79	1999/06/29	12:55:00.371	25
V	Whittier Narrows	14601172	4.44	–118.0817, 33.9923	18.85	282/36/73	2010/03/16	11:04:00.026	187
W	La Habra	15481673	5.10	–117.9300, 33.9220	5.00	239/70/38	2014/03/29	04:09:42.970	312
X	Chino Hills	14383980	5.39	–117.7613, 33.9530	14.70	47/51/32	2008/07/29	18:42:15.960	341
Y	2002 Yorba Linda	9818433	4.75	–117.7758, 33.9173	12.92	34/84/-10	2002/09/03	07:08:51.675	67
Z	2009 Yorba Linda	10399889	3.98	–117.7892, 33.8940	4.23	208/65/26	2009/04/24	03:27:49.840	97
AA	ESE of Yorba Linda	9644101	3.64	–117.6882, 33.8777	3.59	56/65/37	2001/04/13	11:50:11.916	53
AB	Lake Elsinore	10275733	4.73	–117.4770, 33.7322	12.60	65/59/58	2007/09/02	17:29:14.827	118
AC	Westlake Village	10403777	4.42	–118.8825, 34.0667	14.17	254/73/30	2009/05/02	01:11:13.084	100
AD	Hermosa Beach	14738436	3.69	–118.4578, 33.8572	11.23	57/41/54	2010/06/07	23:59:27.165	99

point source the material is homogeneous, we estimated the rise time to be

$$t_r = \frac{16}{7} \frac{l_s f^{0.5}}{V_S \pi^{1.5}} , \tag{1}$$

where f is a shape factor equal to the ratio w_d/l_s, such that $A = f l_s^2$ (e.g. Stein and Wysession, 2003; Shearer, 2009).

Having estimated the rise time, we used the formulation proposed by Tinti et al. (2005) to express the source slip-rate function, $\dot{s}(t)$, as

$$\dot{s}(t) = D \int_{-\infty}^{\infty} W(t-\tau) Y(\tau) d\tau . \tag{2}$$

Here, $W(t)$ and $Y(t)$ are a triangular (smoothing) function and the Yoffe (1951) function, respectively. D is the final (maximum) slip, which we obtained based on the seismic moment of each event, $M_o = \mu D A$. The values of the shear modulus, μ, were extracted from the velocity models ($\mu = \rho V_S^2$) at the corresponding hypocentral locations. In turn, the rise-time associated with the Yoffe function, τ_r, was estimated based on the fact that from eq. (2) we know that the total rise time of the slip-rate function is

$$t_r = \tau_r + 2\tau_s \tag{3}$$

where τ_s is the duration of the triangular function, and t_r corresponds to the value we obtain from eq. (1). For this, in all cases, we assumed a value of $t_s = 0.1 t_r$, which is consistent with some of the tests done by Tinti et al. (2005). The resulting source time functions are shown in Fig. 5.

While we recognize that the procedure just described carries in it significant simplifications—for instance, the database used by Wells and Coppersmith (1994) was limited to earthquakes with a lower bound of M 4.7—we found the slip-rate functions and rise times we obtained to be acceptable. For a handful of events we tested other alternatives and observed the results did not changed significantly, or were better using the chosen procedure. This

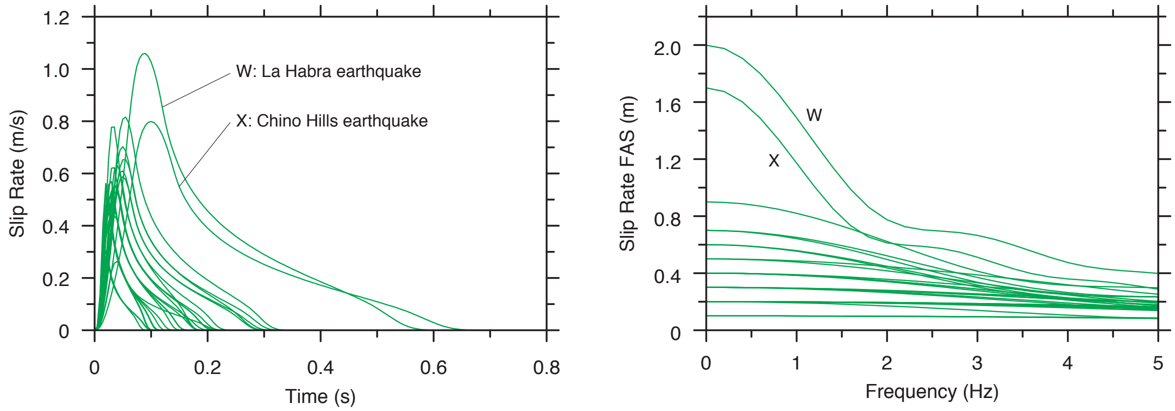

Figure 5: Source slip-rate time functions (left) and Fourier amplitude spectra (bright) of all the events considered. Slip-rate functions were computed based on the total rise time estimated from eqs (1) and (2). The source functions of events W and X, corresponding to the 2014 La Habra and 2008 Chino Hills earthquakes, are singled out in the figure for reference. These two events are the largest of all earthquakes considered.

is due in part to the fact that we are only considering $f_{\max} = 1$ Hz. As it can be seen in Fig. 5, with the exception of the Chino Hills and La Habra earthquakes, the frequency content of the slip-rate functions is nearly flat below 1 Hz, thus any change to the rise time or the shape of the slip functions could only have a marginal effect on the results for earthquakes of the magnitudes considered here.

4 Simulation Approach

We simulated the ground motions for each earthquake and velocity model combination using a 3D finite element approach to solve the anelastic wave equation. Similar numerical methods including finite differences, finite elements, and spectral elements have been successfully used in equivalent problems in the past (e.g. Graves, 1996; Komatitsch and Vilotte, 1998; Bao et al., 1998). In particular, we use a parallel code called Hercules, which implements an octree datastructure for representing unstructured hexahedral meshes in memory and solve the wave equation explicitly in time (Tu et al., 2006; Taborda et al., 2010). Attenuation is introduced by means of a viscoelastic model composed of a set of parallel Maxwell elements and a Voigt element (Bielak et al., 2011), and the absorbing boundaries are modeled using a plane-wave approximation (Lysmer and Kuhlemeyer, 1969). Hercules has been used in multiple verification and validation exercises before, and has shown to be a reliable tool for 3D ground motion simulation (e.g. Bielak et al., 2010; Taborda and Bielak, 2013).

Since none of the velocity models provides information about the quality factors Q_P and Q_S, which are necessary for modeling the effects of intrinsic attenuation effects, we used the Q_S-V_S relationship proposed by Taborda and Bielak (2013) to infer the values of Q_S from the velocity model. This rule is an extension of that introduced by Brocher (2005, 2008), which was in turn inspired by other similar but simpler approximations used in the past (e.g. Olsen et al., 2003; Graves, 2008). Q_P, on the other hand, is derived from the assumption of considering no attenuation due to dilatational deformation, i.e. $Q_\kappa \to \infty$ (e.g., Stein and Wysession, 2003; Shearer, 2009). In both cases we consider the values of Q to remain constant within the range of frequencies considered (for more details, see Bielak et al., 2011).

As mentioned before, we built models in the form of unstructured finite element meshes so that they could represent a maximum frequency, $f_{\max} = 1$ Hz and a minimum shear wave velocity, $V_{S_{\min}} = 200$ m/s. Table 2 describes the main simulation parameters and provides some additional information about performance. All simulations were done on Blue Waters at the National Center for Supercomputing Applications. Table 2 also includes information about the average execution time of the code for every simulation model. Note that the the

Table 2: Simulation parameters.

Numerical parameters	
$f_{\max}$ (Hz)	1.0
$V_{S_{\min}}$ (m/s)	200
Points/wavelength	8–15
Simulation Δt (s)	0.005
Simulation time (s)	100
Number of steps	20,000
Mesh details	
Min. element size (m)	21.97 m
Max. element size (m)	351.56 m
Number elements (mill.)	
CVM-S4	106.4
CVM-S4.26	110.3
CVM-H	249.7
CVM-H+GTL	282.6
Avg. simulation wall-clock time (hr:mm:ss)[b]	
CVM-S4	1:03:46
CVM-S4.26	1:03:58
CVM-H	2:17:24
CVM-H+GTL	2:40:51

[a] The corners of the domains are given in longitude and latitude.

[b] Corresponding to 1,280 cores on NCSA's Blue Waters.

influence of the models CVM-H and CVM-H+GTL having larger areas/volumes of softer deposits is reflected by the number of elements, and consequently, on the time necessary to run each simulation. All simulations considered, we used over 0.27 million of CPU hours.

5 Ground Motion Simulation Results

We first present results from the simulations and discuss the ground motion characteristics. Fig. 6 shows the peak horizontal magnitude of velocity on the free surface for all events, in the particular case of simulations done using the model CVM-S4.26. This figure illustrates how the basins in the region respond to earthquakes originated at various locations within the simulation domain. We observe that earthquakes of magnitude less than 3.9 remain local, showing only a marginal ground response in areas outside their immediate epicentral area (e.g. events L, M, U). Events of magnitude greater than 4.3 show stronger response all throughout the domain, and in the basins (e.g. events D, P, Y). Events with magnitudes between 3.9 and 4.3 are in a transition zone, where the shallower events register stronger ground motions (e.g. events Q and Z).

The largest ground motions are obtained for the 2014 M_w 5.10 La Habra and 2008 M_w 5.39 Chino Hills earthquakes (events W and X, respectively), and the areas with most significant shaking are the greater Los Angeles basin, the San Bernardino basin and the region between Simi valley and the Ventura basin. While Fig. 6 only includes results obtained using CVM-S4.26, these observations are somewhat similar across velocity models, depending on their own crustal distinctions, as illustrated next.

Fig. 7 shows the peak horizontal magnitude of velocity on the free surface for all velocity models, for the particular cases of the 2005 M_w 4.42 Fontana, 2007 M_w 4.66 Chatsworth, and 2014 M_w 5.10 La Habra earthquakes (events G, P, and W, respectively). We select these three events for their location and magnitudes above 4, with well spread response over the simulation domain. The Fontana (G) earthquake epicenter was located in the northern section of the San Jacinto fault zone, not far from the junction with the San Andreas fault zone and the Cucamonga fault (see Fig. 4). This earthquake shows clear influence in the area of the San Bernardino basin for all four models, although with some differences. In the case of CVM-S4, for instance, a significant level of the response is channeled into the Chino and the greater Los Angeles basins, as well as far into the Simi and the Santa Clara river valleys. A similar response is seen in the case of CVM-S4.26, but to a lesser extend, with only marginal response in the Santa Monica area. CVM-S4.26 also exhibits lower values southwest and northwest fromt he epicenter than CVM-S4. In the cases of CVM-H and CVM-H+GTL, the ground motion is more localized around the epicentral area. Both

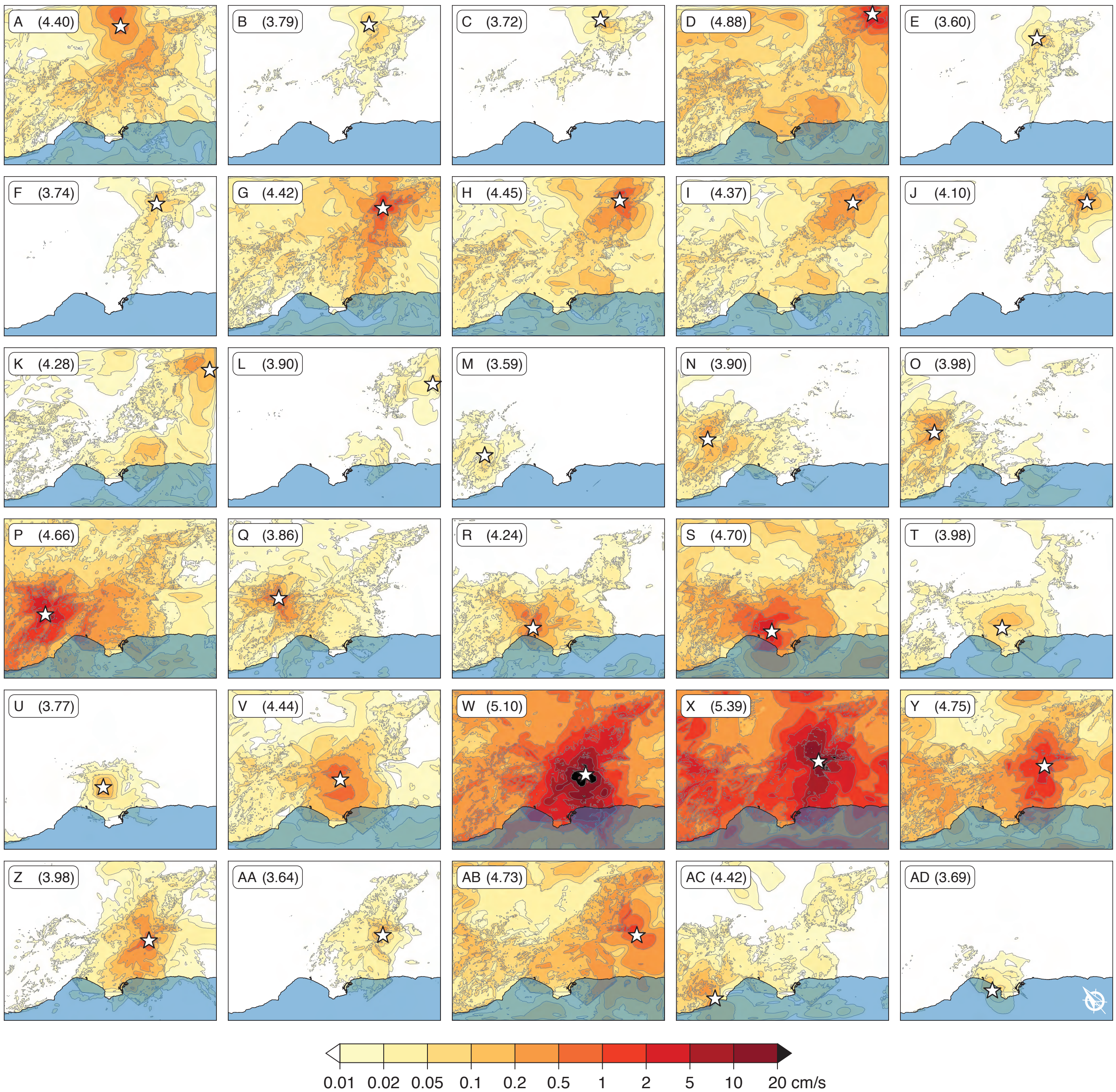

Figure 6: Free surface peak horizontal magnitude velocity from simulations for all the events using the velocity model CVM-S4.26. The letter code used to identify each earthquake is shown at the top-left corner along with the event's magnitude, M_w (see Table 1). In each case, the star indicates the epicenter of the event (see also Fig. 4). Although smaller and larger values than those shown in the color scale were obtained from the simulations, these were truncated for visual convenience.

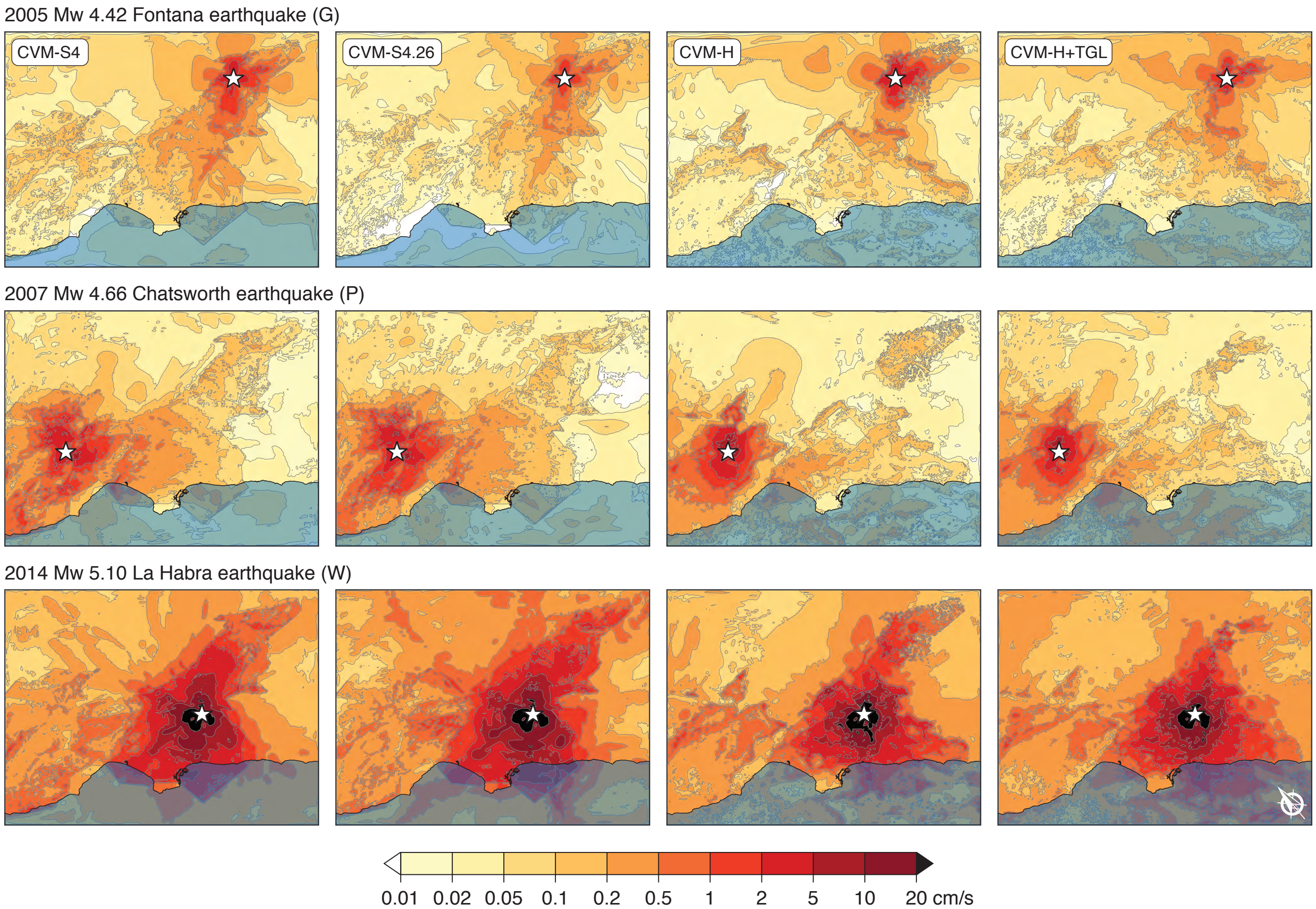

Figure 7: Free surface peak horizontal magnitude velocity for three representative events (from top to bottom: G, W, and P) using all four velocity models (from left to right: CVM-S4, CVM-S4.26, CVM-H and CVM-H+GTL). The stars indicate the epicenter locations (see Table 1 and Fig. 4 for reference). In each case, smaller and larger values than those shown in the contour maps were obtained, but truncated for visual convenience.

models, however, seem to channel more energy along the north flank of the San Andreas Fault and to the south east and south west, in particular along the west edge of the Santa mountains, where both CVM-H and CVM-H+GTL have deeper structures than CVM-S4 or CVM-S4.26 (see Fig. 2 for reference).

In the case of the Chatsworth earthquake, the strongest response concentrates in the Simi and San Fernando valleys, along the Santa Clara river valley and into the Ventura basin. For the simulations done with CVM-S4 and CVM-S4.26, however, a greater amount of energy is channeled west into the Ventura basin and southeast towards the greater Los Angeles area. Both CVM-S4 and CVM-H show some level of basin effects in San Bernardino, an area where CVM-H+GTL shows the least level of amplification of all the models, due to the changes introduced by the GTL model as highlighted in Fig. 3. Both CVM-H and CVM-H+GTL show a stronger contrast between the Simi and San Fernando valleys and the Los Angeles basin, marked by the influence of the Santa Monica mountains, which seem to be more sharply defined in these two models than in CVM-S4 and CVM-S4.26 (see Fig. 2).

Last, in the case of the La Habra earthquake, the ground motions are mostly concentrated in the greater Los Angeles basin, though with some significant differences amongst the models. We first note again the fact that the model CVM-H+GTL introduces strong changes in the response of the San Bernardino basin with respect to CVM-H. As in other cases, CVM-H and CVM-H+GTL yield larger ground motions in the area of Irving (see Fig. 1) southeast from the epicenter. CVM-S4 and CVM-S4.26, on the other hand, exhibit larger ground motions within the Los Angeles basin itself and in the Chino basin. In turn, CVM-S4.26 yields larger shaking near the San Gabriel valley and mountains, and beyond in the Mojave desert. CVM-S4.26 also exhibits stronger response in the area of the Santa Ana mountains, as a result of the contrast in the model in this area with respect to CVM-S4. Of all four models, CVM-S4 has stronger response in the Ventura basin and CVM-H along the Santa Clara river valley—which likely reflects a better coupling between the crustal structure and faults representation in the model, considering the weak zone along the Santa Clara river due to the presence of the Oak Ridge fault beneath it.

Although not in equal measure for all events, the differences just highlighted were common among the models in the simulation results of other earthquakes. We further analyze the implications of these model discrepancies and their consequence in simulation results through the validation of synthetics against data in the following sections.

6 Evaluation Approach

We evaluate the accuracy of the simulations, and thus that of the velocity models, based on a quantitative validation of the simulated ground motions. The validation process consists of comparisons between synthetics and data, at locations where records were available for the simulated events. For this, we compiled a large collection of broadband and strong-motion records from two data centers, the Southern California Earthquake Data Center (SCEDC) and the Center for Engineering Strong Motion Data (CESMD). SCEDC and CESMD archive records from various seismic networks in the southern California region. In total we obtained records from more than 800 stations spread throughout the simulation domain. Unfortunately, not all the stations recorded all the events, thus the number of available data-points for comparisons varies between events.

Records from SDEDC and CESMD were processed depending on the recording station characteristics. In general, we favored working with strong motion records (accelerations) in raw format. We performed gain and baseline corrections, and applied a high-pass filter at 0.05 Hz before integrating to obtain velocities and displacements. Although the majority of stations have instruments oriented as positive in the North (NS), East (EW), and up directions (UD), we rotated the signals if necessary to bring them all to standard orientations. In general, we gave priority to V1 files from CESMD and HN channels from SCEDC, but when otherwise not available we also used V2 files from CESMD and BH channels from SCEDC. In the case of BH channels (broadband velocities) we took derivatives to obtain accelerations and integrated the signals to obtain displacements.

Once we processed all data and synthetics we proceeded with the validation of the simulations for each event, and each velocity model. The validation process was carried out using the goodness-of-fit (GOF) method proposed by Anderson (2004), with minor modifications introduced by Taborda and Bielak (2013). This method compares synthetics against data using eleven individual parameters, namely: Arias integral (C1), energy integral (C2), Arias intensity (C3), total energy (C4), peak acceleration (C5), peak velocity (C6), peak displacement (C7), response spectrum (C8), Fourier amplitude spectrum (C9), cross correlation (C10), and strong-phase duration (C11). Each parameter is mapped onto a numerical scale ranging from 0 to 10, where a score of 10 corresponds to a perfect match between two signals. The eleven scores are combined using the following expression:

$$\mathrm{S} = \frac{1}{9}\left(\frac{\mathrm{C1}+\mathrm{C2}}{2} + \frac{\mathrm{C3}+\mathrm{C4}}{2} + \sum_{i=5}^{11} \mathrm{C}i\right) , \tag{4}$$

and computed for each pair of signals. For the comparisons, both the synthetics and the records are band-pass filtered between 0.1 and 1.0 Hz. The upper limit is determined by the maximum frequency of the simulations. The lower limit is determined by the need of limiting numerical errors introduced when processing strong motion (acceleration) and broadband (velocity) records to obtain either velocities and displacements. This also helps in eliminating permanent displacements in records near the epicenter (especially for shallower earthquakes) in the synthetics, given that these are not captured in the records. THe GOF scores are run over the processed pair of signals not only for the 0.1–1.0 Hz bandwidth (here identified ans the “broadband” set, or BB) but also for three additional bandwidths following the guidelines suggested by Anderson (2004). These are SB_1 (0.1–0.25 Hz), SB_2 (0.25–0.5 Hz), SB_3 (0.5–1 Hz). The results of S from equation (4) for the broadband and each of the individual bands analysis are then combined to obtain a final score (FS), define as:

$$\text{FS} = \frac{1}{6}\left(\text{BB} + \sum_{i=1}^{5}\text{SB}_i\right) . \tag{5}$$

Additional details about the original parameters proposed by Anderson (2004) and the modifications introduced to the scoring criterion are given in Taborda and Bielak (2013), where we also discuss our preference of Anderson's procedure over other available methods such as those of Kristeková et al. (2009) or Olsen and Mayhew (2010). We favor Anderson (2004) because its metrics convey physical meaning to both seismologists and engineers, and because it suits best the validation of synthetics with respect to data—as opposed to Kristeková et al. (2009), which works best for verification purposes. Olsen and Mayhew (2010), on the other hand, is in many respects equivalent to Anderson (2004).

7 Evaluation Results

After simulations results were obtained, we computed the GOF scores as described in the previous section for all event simulations, for all velocity models. Figures 8 and 9 show results of the final score (FS, equation 5) obtained for a selection of events (10 out of 30). These events are a subset of 12 events for which we had more than 100 stations with records (see last column in Table 1). Given the fact that GOF scores are local to each station, it should be recognized that the contours drawn for visual interpretation should in all rigor not be understood as representative of intermediate areas between the stations, but merely as a first approximation to understand the accuracy of the models to represent the ground motion over the entire region of interest. The histograms at the bottom of each map indicate the count of stations with a FS value in a 0.5-bin width in the GOF scale from 0 to 10.

Overall, the GOF scores range between values as low as 0.5 and as high as 8.5. Although the histograms do not exhibit any particular statistical distribution, most values tend to conglomerate in the ranges between 3 and 7. While a more detailed analysis will require investigating any correlation between the crustal structure and/or the near-surface geotechnical layer properties, from these figures it is difficult to conclude with certainty if there is any spatial correlation in the distribution of the scores, and or its relationship with epicentral locations. This will be the subject of further analysis beyond the scope of the project plan. On the other hand, these results do facilitate understanding the overall accuracy of the models across a large number of simulations, as done here.

Figure 10, for instance, summarizes these results for all events and all models. This figure shows the averages of FS values across all the validation stations for each event and compares the results of such averages for the different velocity models. The average scores oscillate between values of 2.5 and 6.5, with most values above 3.5. These results indicate that, overall, the velocity model CVM-S4.26 leads to the best results in 20 out of the 30 events considered in this project. On the other hand, this model only leads to the worst score in two events (A and AC). The events with the best scores for CVM-S4.26 are events B, N, T, X. So far, we have not yet identified any trend in terms of umber of validation stations with the scores. Events, with similar amounts of data available are apparently as prone to lead to good scores as bad ones, as it can be seen in the contrast between events R and AB in Figs 8 and 9.

Alternatively, these results can be discretized or disaggregated in terms of frequency bands. Figure 11 shows the averages of each event for the different frequency bands used in the validation procedure. Two aspects are of importance here. First, that the trend for almost all events is maintained across different frequency bands. That is, when an event exhibits a higher score with respect to other events, or when a model leads to a better score with respect to other models, in most cases, such condition is maintained across the different bandwidths of analysis. Second, that overall, the higher the frequency range, the lower the score. The second of these observations is consistent with expectations and observations from other validation efforts which have indicated that our capacity to reproduce the ground motions is better at the lower frequencies than at the higher ones. On the other hand, the first of these observations is very important in the sense that these results indicate that improvements in the lower

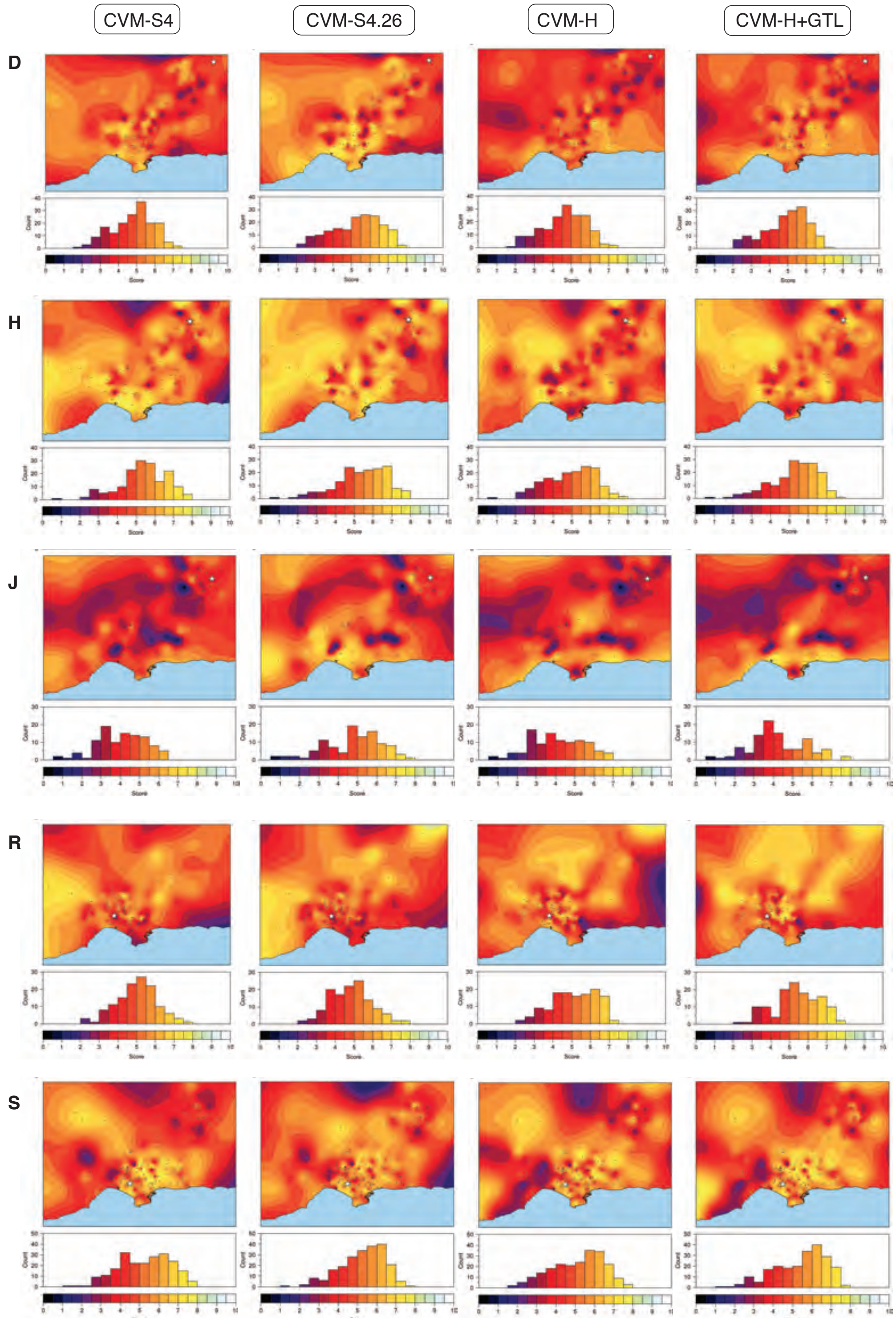

Figure 8: Goodness of fit (final score, FS) maps for selected events D, H, J, R, and S, for all models (from left to right: CVM-S4, CVM-S4.26, CVM-H, and CVM-H+GTL). These are events with more than 100 stations used for validations. The color scale indicates the GOF obtained at each station (black dots). The contour are smoothed over the available scores from the stations over the entire region, although values remain a local measure of the fit. The star indicates the location of the epicenter, and the event code (see Table 1) is indicated on the left margin.

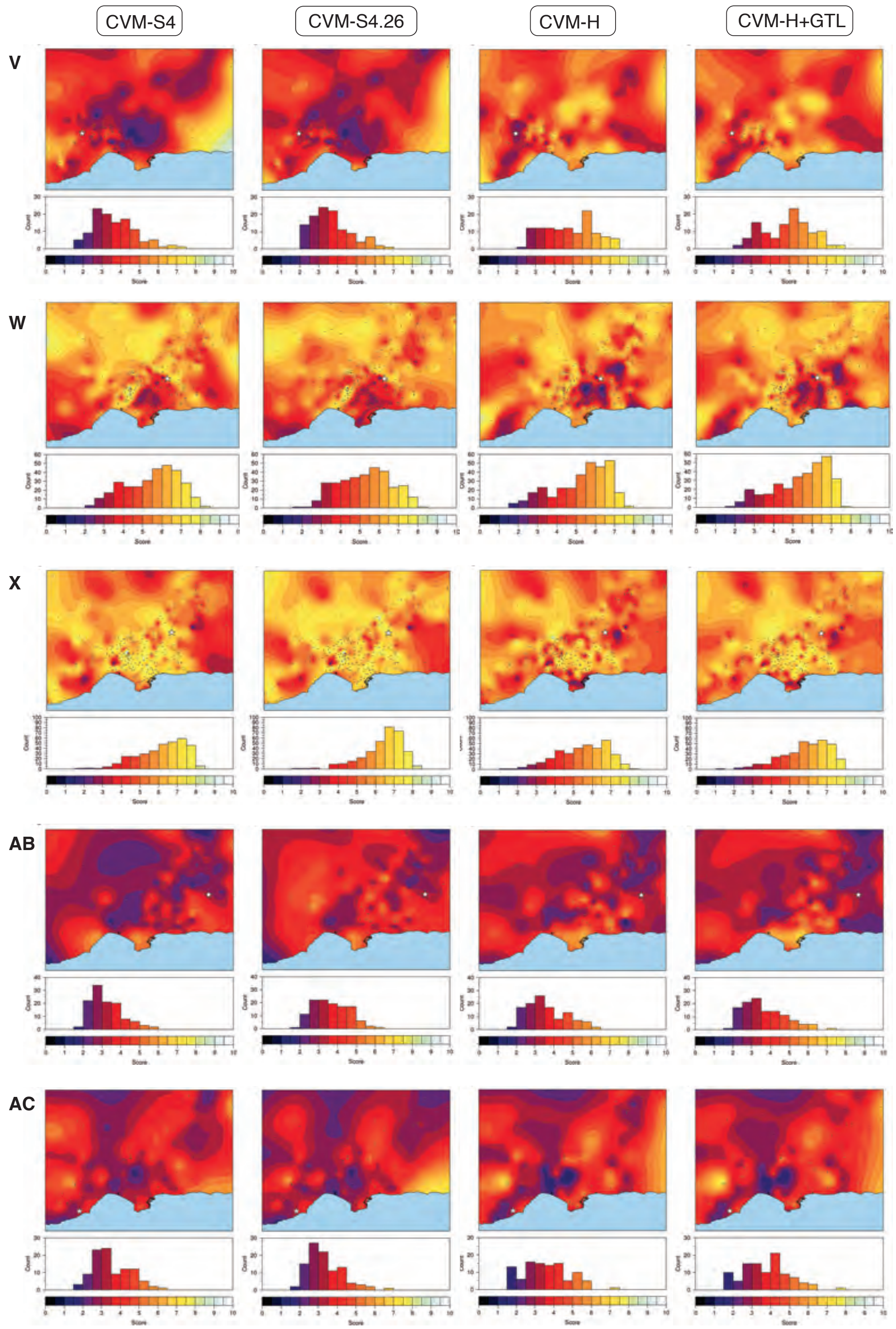

Figure 9: Same as Fig 8, but for events V, W, X, AB and AC. These events also had more than 100 stations available for validations. The color scale indicates the GOF obtained at each station (black dots). The contour are smoothed over the available scores from the stations over the entire region, although values remain a local measure of the fit. The star indicates the location of the epicenter, and the event code (see Table 1) is indicated on the left margin.

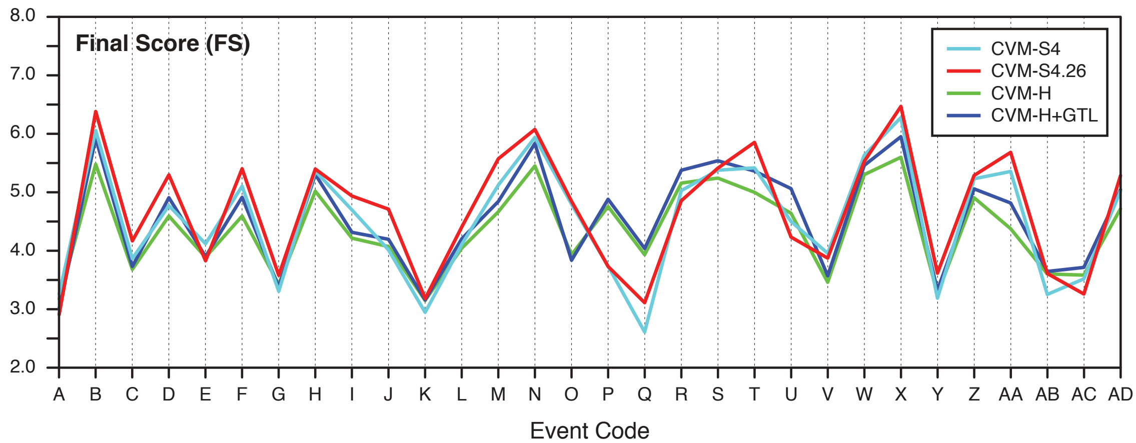

Figure 10: Summary of average final scores (FS) for all events. Values for each event are the average of the FS for all validation stations available for that event. Different color lines indicate the velocity model used for the corresponding simulations.

frequency ranges propagate over higher frequencies as well. The reason we stress on this observations is because this indicates that recent efforts in full three-dimensional tomography (inversions) have a positive impact on improving the accuracy of models even for simulations done at frequencies higher than those of the inversions done to update the velocity model. In other words, CVM-S4.26 is a better model than CVM-S4, not only in the frequency ranges up to 0.2 Hz (which was the maximum frequency for the inversion), but also at the higher frequency bands.

The results shown in Figures 10 and 11 also indicate that the inclusion of a geotechnical model to smooth the near surface profiles has, overall, a positive impact on the results obtained with CVM-H+GTL over those obtained using CVM-H (without the GTL module). Such conclusion is equally consistent across events, but seems to increase with frequency, as expected from the fact that the GTL model is very shallow with respect to the depth scale of the simulation domain, and thus it should play a more significant role at the higher frequencies (as wavelengths become shorter and shorter). This, however, should be taken carefully, as previous studies (Taborda and Bielak, 2014) have shown that the GTL model, as currently implemented in the UCVM platform and the CVM-H software, can significantly alter the velocity contrasts between basins and bedrock.

Las, we present further condensed results for each model over the entire region. Figure 12 shows average GOF results for each velocity model. Here, the average score at each station location is computed only among those events with more than 100 validation stations, and when 7 or more events recorded the ground motion at the same station. In total, 90 stations recorded the ground motions of 7 or more events. This figure, then, shows the average FS values for such criteria. The first aspect to highlight from Figure 12 is the uniformity of the results obtained for CVM-S4.26. While the values are not necessarily higher than in other cases (most stations score within the bin of 4.5–5.0), this reflects the fact that this model leads to the most consistent results across the region of interest. It also reflects the improvements obtained as one transitions from CVM-S4 to CVM-S4.26. That is, in the histogram, a portion of the counts of stations scoring values lower than 4.5 are moved up to the 4.5–5.0 bin. Yet the ones above 5.0 remain unchanged.

The other aspect to highlight in Figure 12 is the fact that the histogram in CVM-H+GTL has a slight shift in the count of station scores to the right. That is, lower counts below 4.5 and hight counts above 5.0 with respect to the case of CVM-H. This, again, reflects on the positive effect of including the GTL model in the computations. In addition, the comparisons in this figure seem to indicate that both the CVM-S models (4 and 4.26) need to be improved in the region south-east from the Chino and San Bernardino basins, as this seems to be an area where the stations a that location scored lower than the rest. Same applies for the CVM-H models in the region of the Santa

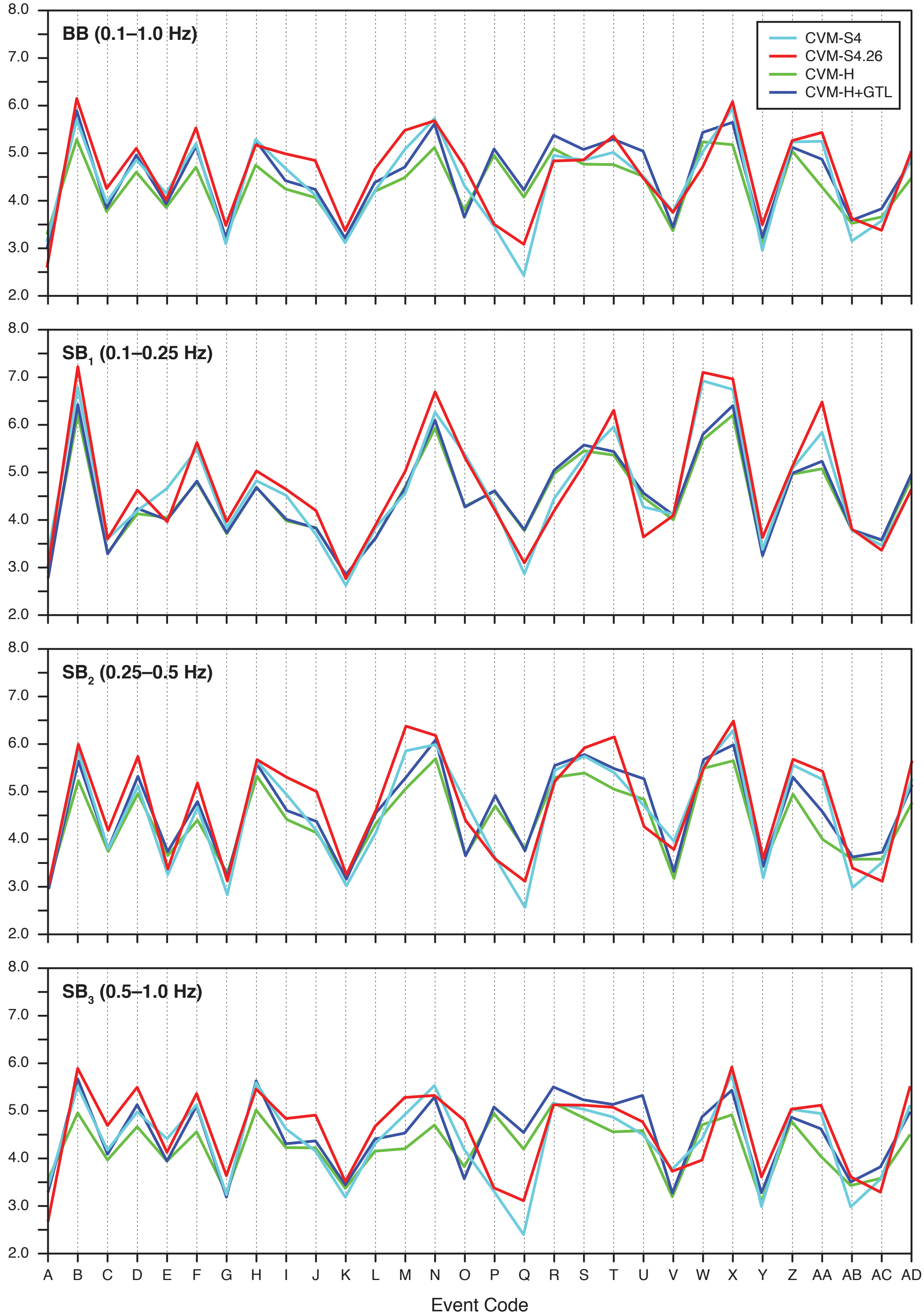

Figure 11: Average score per frequency band, discretized in terms of frequency bands, for the broadband case (BB), and the three additional low-to-high bandwidths (SB_i). Values for each event are the average of the FS for all validation stations available for that event, in each of the given bandwidths. Different color lines indicate the velocity model used for the corresponding simulations.

Monica mountains along the shore line between Los Angeles and Oxnard. This could in part be a topography effect in the simulations, which would required additional analysis in the future.

8 Concluding Remarks

This project obtained validation results for a series of simulations of historical earthquakes using the various velocity models available for southern California, with the objective of drawing conclusions about the effectiveness of these models to reproduce the ground motions in the vicinity of the greater Los Angeles basin and metropolitan area. The results indicate that, for the events considered and given the simplifications in terms of the source representations, the velocity model leading to the best fitting results is CVM-S4.26. We obtained goodness-of-fit scores to compare synthetics and data and conducted an analysis over different frequency bands, and in all cases the results were consistent in this conclusion. More important, the results indicated that this model led to more accurate results even at frequencies beyond those for which the model was originally intended. Although more evaluations in the future will be necessary, this supports current efforts in full three-dimensional tomographic inversions being done by other researchers to improve existing and develop new velocity models. It also provides a basis for supporting higher frequency simulations above the limits typically understood as valid from inversion results.

Future efforts will need to be dedicated to analysis of validation results in light of the properties and characteristics of the model and the ground motion. Aspects that were not considered within the project plan of this investigation included the parameters of the attenuation model used to represent internal friction in the material (Q_S-V_S and Q_P-Q_S relationships) or the potential changes in material properties due to large deformations during stronger, larger magnitude events. We will also need to explore potential correlations between the observed goodness-of-fit scores and source parameters, epicentral distance, basin depth, and site effects. These and other aspects are the subject of current effort in our research group.

References

Anderson, J. G. (2004). Quantitative measure of the goodness-of-fit of synthetic seismograms. In *Proc. 13th World Conf. on Earthquake Eng.*, Vancouver, British Columbia, Canada. Int. Assoc. Earthquake Eng. Paper 243.

Azizzadeh-Roodpish, S., Khoshnevis, N., and Taborda, R. (2014). Evaluation of the southern california velocity models through simulation and validation of multiple historical events. In *Proc. SCEC Annu. Meet.*, number CME 080, Palm Springs, CA, September 6–10.

Azizzadeh-Roodpish, S., Taborda, R., Khoshnevis, N., and Cheng, K. (2015). Evaluation of the scec seismic velocity models through simulation and validation of past earthquakes. In *Proc. SCEC Annu. Meet.*, number CME 037, Palm Springs, CA, September 12–16.

Bao, H., Bielak, J., Ghattas, O., Kallivokas, L. F., O'Hallaron, D. R., Shewchuk, J. R., and Xu, J. (1998). Large-scale simulation of elastic wave propagation in heterogeneous media on parallel computers. *Comput. Meth. Appl. Mech. Eng.*, 152(1-2):85–102.

Bielak, J., Graves, R. W., Olsen, K. B., Taborda, R., Ramírez-Guzmán, L., Day, S. M., Ely, G. P., Roten, D., Jordan, T. H., Maechling, P. J., Urbanic, J., Cui, Y., and Juve, G. (2010). The ShakeOut earthquake scenario: Verification of three simulation sets. *Geophys. J. Int.*, 180(1):375–404.

Bielak, J., Karaoglu, H., and Taborda, R. (2011). Memory-efficient displacement-based internal friction for wave propagation simulation. *Geophysics*, 76(6):T131–T145.

Brocher, T. M. (2005). Compressional and shear wave velocity versus depth in the San Francisco bay area, California: Rules for USGS Bay Area Velocity Model 05.0.0. Technical Report OFR-2005-1317, U.S. Geological Survey.

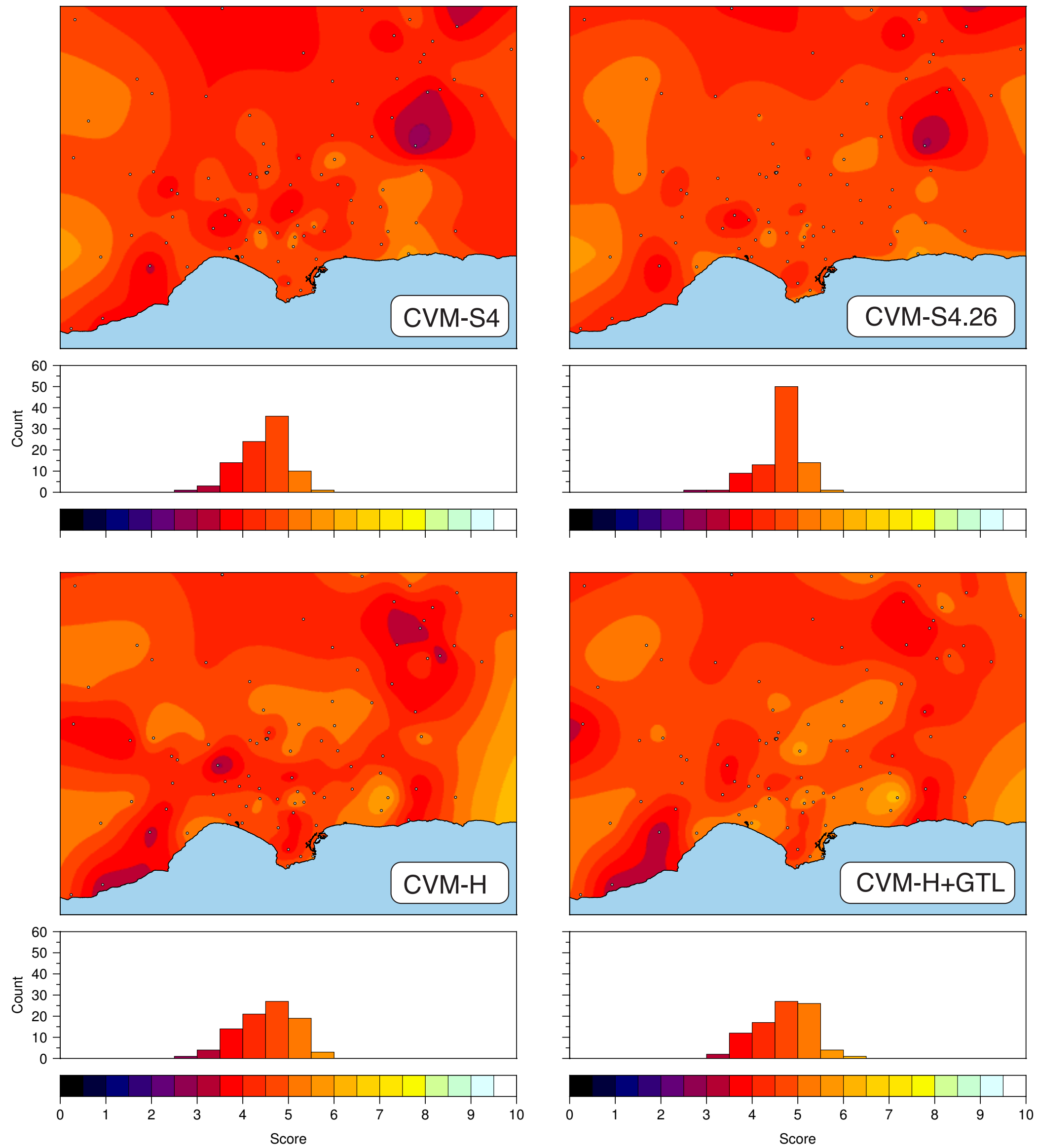

Figure 12: Average goodness-of-fit maps for each velocity model based on results from events with at least 100 validation stations. The average final score at each station was obtained provided that at least 7 or more events had the same station in common.

Brocher, T. M. (2008). Compressional and shear-wave velocity versus depth relations for common rock types in northern California. *Bull. Seismol. Soc. Am.*, 98(2):950–968.

Brocher, T. M., Aagaard, B. T., Simpson, R. W., and Jachens, R. C. (2006). The USGS 3D seismic velocity model for northern California. *Eos Trans. AGU*, 87(52): Fall Meet. Suppl., Abstr. S51B–1266.

Chaljub, E., Moczo, P., Tsuno, S., Bard, P.-Y., Kristek, J., Kaser, M., Stupazzini, M., and Kristekova, M. (2010). Quantitative comparison of four numerical predictions of 3D ground motion in the Grenoble Valley, France. *Bull. Seismol. Soc. Am.*, 100(4):1427–1455.

Chen, P., Zhao, L., and Jordan, T. H. (2007). Full 3D tomography for the crustal structure of the Los Angeles region. *Bull. Seismol. Soc. Am.*, 97(4):1094–1120.

Ely, G. P., Jordan, T. H., Small, P., and Maechling, P. J. (2010). A Vs30-derived near-surface seismic velocity model. In *Abstr. AGU Fall Meet.*, number S51A-1907, San Francisco, California, December 13–17.

Fujiwara, H., Kawai, S., Aoi, S., Morikawa, N., Senna, S., Kudo, N., Ooi, M., Hao, K. X.-S., Hayakawa, Y., Toyama, N., Matsuyama, N., Iwamoto, K., Suzuki, H., and Ei, R. (2009). A study on subsurface structure model for deep sedimentary layers of Japan for strong-motion evaluation. Technical Report 337, National Research Institute for Earth Science and Disaster Prevention, Tsukuba, Japan, (in Japanese).

Gill, D., Small, P., Taborda, R., Lee, E.-J., Olsen, K. B., Maechling, P. J., and Jordan, T. H. (2015). Standardized access to seismic velocity models using the unified community velocity model (UCVM) software. In *Abstr. SSA Annu. Meet.*, Pasadena, California, 21–23 April. Accepted.

Graves, R. W. (1996). Simulating seismic wave propagation in 3D elastic media using staggered-grid finite differences. *Bull. Seismol. Soc. Am.*, 86(4):1091–1106.

Graves, R. W. (2008). The seismic response of the San Bernardino basin region during the 2001 Big Bear lake earthquake. *Bull. Seismol. Soc. Am.*, 98(1):241–252.

Hauksson, E. (2000). Crustal structure and seismicity distribution adjacent to the Pacific and North America plate boundary in southern California. *J. Geophys. Res.*, 105(B6):13,875–13,904.

Kohler, M. D., Magistrale, H., and Clayton, R. W. (2003). Mantle heterogeneities and the SCEC reference three-dimensional seismic velocity model version 3. *Bull. Seismol. Soc. Am.*, 93(2):757–774.

Koketsu, K., Miyake, H., Fujiwara, H., and Tashimoto, T. (2008). Progress towards a Japan integrated velocity structure model and long-period ground motion hazard map. In *Proc. 14th World Conf. Earthquake Eng.*, number S10-038, page 7, October 12–17, Beijing, China.

Komatitsch, D. and Vilotte, J.-P. (1998). The spectral element method: An efficient tool to simulate the seismic response of 2D and 3D geological structures. *Bull. Seismol. Soc. Am.*, 88(2):368–392.

Kristeková, M., Kristek, J., and Moczo, P. (2009). Time-frequency misfit and goodness-of-fit criteria for quantitative comparison of time signals. *Geophys. J. Int.*, 178(2):813–825.

Lee, E.-J., Chen, P., and Jordan, T. H. (2014a). Testing waveform predictions of 3d velocity models against two recent los angeles earthquakes. *Seismol. Res. Lett.*, 85(6):1275–1284.

Lee, E.-J., Chen, P., Jordan, T. H., Maechling, P. J., Denolle, M., and Beroza, G. C. (2014b). Full-3-D tomography for crustal structure in southern California based on the scattering-integral and the adjoint-wavefield methods. *J. Geophys. Res.*, 119(8):6421–6451.

Lee, E.-J., Chen, P., Jordan, T. H., and Wang, L. (2011). Rapid full-wave centroid moment tensor (CMT) inversion in a three-dimensional earth structure model for earthquakes in Southern California. *Geophys. J. Int.*, 186(1):311–330.

Lysmer, J. and Kuhlemeyer, R. L. (1969). Finite dynamic model for infinite media. *J. Eng. Mech. Div., ASCE*, 95(EM4):859–877.

Magistrale, H., Day, S., Clayton, R. W., and Graves, R. (2000). The SCEC southern California reference three-dimensional seismic velocity model version 2. *Bull. Seismol. Soc. Am.*, 90(6B):S65–S76.

Magistrale, H., McLaughlin, K., and Day, S. (1996). A geology-based 3D velocity model of the Los Angeles basin sediments. *Bull. Seismol. Soc. Am.*, 86(4):1161–1166.

Magistrale, H., Olsen, K. B., and Pechmann, J. C. (2006). Construction and verification of a Wasatch front community velocity model. Technical Report 06HQGR0012, U.S. Geological Survey.

Manakou, M. V., Raptakis, D. G., Chávez-García, F. J., Apostolidis, P. I., and Pitilakis, K. D. (2010). 3D soil structure of the Mygdonian basin for site response analysis. *Soil Dynam. Earthquake Eng.*, 30(11):1198–1211.

Maufroy, E., Chaljub, E., Hollender, F., Kristek, J., Moczo, P., Klin, P., Priolo, E., Iwaki, A., Iwata, T., Etienne, V., De Martin, F., Theodoulidis, N. P., Manakou, M., Guyonnet-Benaize, C., Pitilakis, K., and Bard, P.-Y. (2015). Earthquake ground motion in the Mygdonian basin, Greece: The E2VP verification and validation of 3D numerical simulation up to 4 Hz. *Bull. Seismol. Soc. Am.*, 105(3):1398–1418.

Olsen, K. B. (1994). *Simulation of three-dimensional wave propagation in the Salt Lake basin.* PhD thesis, University of Utah, Salt Lake City, Utah.

Olsen, K. B., Day, S. M., and Bradley, C. R. (2003). Estimation of Q for long-period (> 2 sec) waves in the Los Angeles basins. *Bull. Seismol. Soc. Am.*, 93(2):627–638.

Olsen, K. B. and Mayhew, J. E. (2010). Goodness-of-fit criteria for broadband synthetic seismograms, with application to the 2008 M_{w} 5.4 Chino Hills, California, earthquake. *Seismol. Res. Lett.*, 81(5):715–723.

Plesch, A., Shaw, J. H., Hauksson, E., and Tanimoto, T. (2008). SCEC community velocity model (CVM-H 5.5). In *Proc. SCEC Annu. Meet.*

Plesch, A., Suess, M. P., Munster, J., Shaw, J. H., Hauksson, E., Tanimoto, T., and Members of the USR Working Group (2007). A new velocity model for southern California: CVM-H 5.0. In *Proc. SCEC Annu. Meet.*, Palm Springs, CA, September 8–12.

Plesch, A., Tape, C., Graves, R., Shaw, J., Small, P., and Ely, G. (2011). Updates for the CVM-H including new representations of the offshore Santa Maria and San Bernardino basin and a new Moho surface. In *Proc. SCEC Annu. Meet.*, number B-128.

Plesch, A., Tape, C., Shaw, J. H., and Members of the USR Working Group (2009). CVM-H 6.0: Inversion integration, the San Joaquin valley and other advances in the community velocity model. In *Proc. SCEC Annu. Meet.*, Palm Springs, CA, September 13–16.

Prindle, K. and Tanimoto, T. (2006). Teleseismic surface wave study for S-wave velocity structure under an array: Southern California. *Geophys. J. Int.*, 166(2):601–621.

Ramírez-Guzmán, L., Boyd, O. S., Hartzell, S., and Williams, R. A. (2012). Seismic velocity model of the Central United States (Version 1): Description and simulation of the 18 April 2008 Mt. Carmel, Illinois, earthquake. *Bull. Seismol. Soc. Am.*, 102(6):2622–2645.

Schlosser, S. W., Ryan, M. P., Taborda, R., López, J., O'Hallaron, D., and Bielak, J. (2008). Materialized community ground models for large-scale earthquake simulation. In *SC'08: Proc. ACM/IEEE Int. Conf. for High Performance Computing, Networking, Storage and Analysis*, page 11, Austin, Texas. IEEE Computer Society.

Shaw, J. H., Plesch, A., Tape, C., Suess, M. P., Jordan, T. H., Ely, G., Hauksson, E., Tromp, J., Tanimoto, T., Graves, R., Olsen, K., Nicholson, C., Maechling, P. J., Rivero, C., Lovely, P., Brankman, C. M., and Munster, J. (2015). Unified structural representation of the southern California crust and upper mantle. *Earth Planet. Sci. Lett.*, 415:1–15.

Shearer, P. M. (2009). *Introduction to Seismology.* Cambridge University Press.

Small, P., Maechling, P., Jordan, T., Ely, G., and Taborda, R. (2011). SCEC UCVM — Unified California velocity model. In *Abstr. AGU Fall Meet.*, number S21B-2200, San Francisco, California, December 5–9.

Stein, S. and Wysession, M. (2003). *An introduction to seismology, earthquakes, and earth structure.* Wiley-Blackwell.

Süss, M. P. and Shaw, J. H. (2003). *P* wave seismic velocity structure derived from sonic logs and industry reflection data in the Los Angeles basin, California. *J. Geophys. Res.*, 108(B3):2170.

Taborda, R., Azizzadeh-Roodpish, S., Khoshnevis, N., and Cheng, K. (2016). Evaluation of the southern California seismic velocity models through simulation and validation of historical events. *Geophys. J. Int.* Manuscript in preparation (to be submitted October 2015).

Taborda, R. and Bielak, J. (2013). Ground-motion simulation and validation of the 2008 Chino Hills, California, earthquake. *Bull. Seismol. Soc. Am.*, 103(1):131–156.

Taborda, R. and Bielak, J. (2014). Ground-motion simulation and validation of the 2008 Chino Hills, California, earthquake using different velocity models. *Bull. Seismol. Soc. Am.*, 104(4):1876–1898.

Taborda, R., López, J., Karaoglu, H., Urbanic, J., and Bielak, J. (2010). Speeding up finite element wave propagation for large-scale earthquake simulations. Technical Report CMU-PDL-10-109, Carnegie Mellon University, Parallel Data Lab.

Taborda, R., López, J., O'Hallaron, D., Tu, T., and Bielak, J. (2007). A review of the current approach to CVM-Etrees. In *Proc. SCEC Annu. Meet.*, Palm Springs, CA, September 8–12.

Tape, C., Liu, Q., Maggi, A., and Tromp, J. (2009). Adjoint tomography of the southern California crust. *Science*, 325(5943):988–992.

Tape, C., Liu, Q., Maggi, A., and Tromp, J. (2010). Seismic tomography of the southern California crust based on spectral-element and adjoint methods. *Geophys. J. Int.*, 180(1):433–462.

Tinti, E., Fukuyama, E., Piatanesi, A., and Cocco, M. (2005). A kinematic source-time function compatible with earthquake dynamics. *Bull. Seismol. Soc. Am.*, 95(4):1211–1223.

Tromp, J., Tape, C., and Liu, Q. (2005). Seismic tomography, adjoint methods, time reversal and banana-doughnut kernels. *Geophys. J. Int.*, 160(1):195–216.

Tu, T., López, J., and O'Hallaron, D. (2003). The etree library: A system for manipulating large octrees on disk. Technical Report CMU-CS-03-174, School of Computer Science, Carnegie Mellon University, Pittsburgh, Pennsylvania.

Tu, T., Yu, H., Ramírez-Guzmán, L., Bielak, J., Ghattas, O., Ma, K.-L., and O'Hallaron, D. R. (2006). From mesh generation to scientific visualization: An end-to-end approach to parallel supercomputing. In *SC '06: Proc. ACM/IEEE Int. Conf. for High Performance Computing, Networking, Storage and Analysis*, page 15, Tampa, Florida. IEEE Computer Society.

Wald, D. J. and Allen, T. I. (2007). Topographic slope as a proxy for seismic site conditions and amplification. *Bull. Seismol. Soc. Am.*, 97(5):1379–1395.

Wells, D. L. and Coppersmith, K. J. (1994). New empirical relationships among magnitude, rupture length, rupture width, rupture area, and surface displacement. *Bull. Seismol. Soc. Am.*, 84(4):974–1002.

Wills, C. J. and Clahan, K. B. (2006). Developing a map of geologically defined site-condition categories for California. *Bull. Seismol. Soc. Am.*, 96(4A):1483–1501.

Yoffe, E. H. (1951). The moving griffith crack. *Phil. Mag.*

Zhao, L., Jordan, T. H., Olsen, K. B., and Chen, P. (2006). Fréchet kernels for imaging regional earth structure based on three-dimensional reference models. *Bull. Seismol. Soc. Am.*, 95(6):2066–2080.

Evaluation of the Southern California Velocity Models through Simulation and Validation of Multiple Historical Events

Shima Azizzadeh-Roodpish,[1] Naeem Khoshnevis,[2] Ricardo Taborda,[1,2]

1 Department of Civil Engineering, The University of Memphis
2 Center for Earthquake Research and Information, The University of Memphis

Abstract

We conduct a series of simulations for multiple historical moderate-magnitude earthquakes and validate our results against recorded data to evaluate the velocity models available for southern California. SCEC supports two main community velocity models for the region, namely CVM-S and CVM-H. Both models offer different possibilities or variations, which can be accessed via the SCEC UCVM Platform. CVM-S, for instance, can be queried in its original version (CVM-S4), or with modifications recently included after a 3D tomographic inversion study (CVM-S4.26). The information in CVM-H, on the other hand, can be alternatively used with a supplemental geotechnical model (GTL) or without it. One can therefore produce two different models, CVM-H+GTL (i.e., CVM-H with the GTL model) or (i.e., without it). We performed multiple simulations of earthquakes with magnitudes varying between 3.5 and 5.5 using the four models just described (CVM-S4, CVM-S4.26, CVM-H, and CVM-H+GTL). The simulations were done for a maximum frequency of 1 Hz and a minimum shear wave velocity of 200 m/s using Hercules, an octree-based finite-element parallel earthquake ground motion simulator. The earthquake ruptures were modeled assuming a kinematic point-source (double-couple) representation. Synthetics on about 50 stations per event were compared with data recorded during the earthquakes and downloaded from the Southern California Earthquake Data Center. The seismograms were processed and compared with the synthetics in the range of 0.1--1.0 Hz using a modified version of the Anderson Goodness-of-Fit (GOF) method. This method combines various comparison criteria that are meaningful to both engineers and seismologists, and has been satisfactorily used in previous validation efforts. We compare the regional distribution of the GOF results for all the earthquakes and all the models and draw conclusions on the consistency observed in the results.

Project Concept

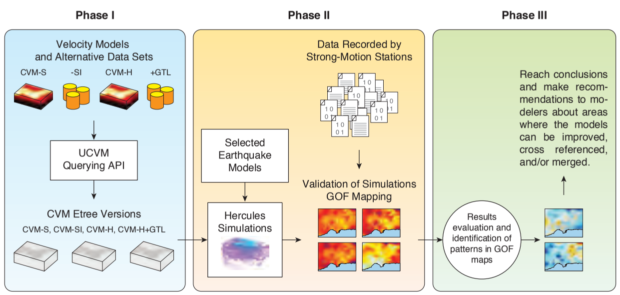

The project's concept is organized in three phases. In the first phase we buit materialized models of the available crustal velocity models for the region of southern California suitable for simulations using Hercules, a highly scalable end-to-end ground motion simulation engine part of the SCEC High-F platform. In the second phase we perform simulations for selected earthquakes and process data available for these events to conduct individual validation studies. And in the third phase, to be completed, we will analyze the results from the multiple validations and models to identify possible patterns that can lead to recommendations on how to improve models and simulations.

Selected Events

Event ID	Mw	Strike	Dip	Rake	Year	MM	DD	Lon	Lat	Depth
A: 9716853	3.98	116	68	71	2001	10	28	-118.27	33.93	21.13
B: 9753489	3.9	83	62	57	2002	1	29	-118.67	34.37	14.21
C: 10275733	4.73	65	59	58	2007	9	2	-117.48	33.73	12.60
D: 10370141	4.45	87	70	28	2009	1	9	-117.30	34.11	14.22
E: 10399889	3.98	208	65	26	2009	4	24	-117.79	33.89	4.23
F: 10403777	4.42	254	73	30	2009	5	2	-118.88	34.07	14.17
G: 10972299	3.79	98	58	68	2001	7	19	-117.46	34.27	10.91
H: 14312160	4.66	82	27	51	2007	8	9	-118.62	34.30	7.58
I: 14383980	5.39	47	51	32	2008	7	29	-117.76	33.95	14.70
J: 15237281	3.86	236	58	33	2012	10	28	-118.46	34.35	3.59

Region of Interest

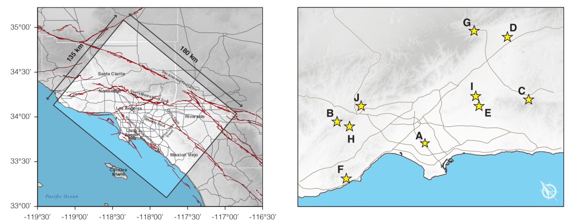

We consider a set of 10 events in a simulation domain with a surface area of 180 km x 135 km. The simulation domain covers all major basins in the greater Los Angeles region. The events vary in magnitude between 3.7 and 5.4, and were all modeled using a point source representation.

Velocity Models

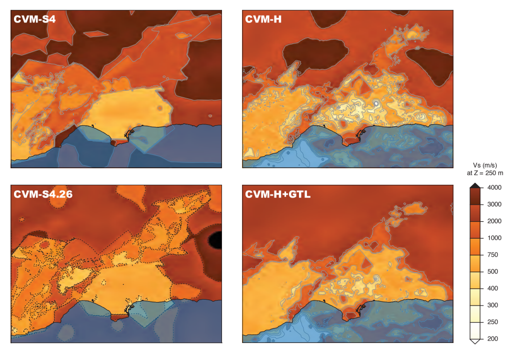

The simulations of the selected events are all done for the four major velocity models currently available for the region of southern California: CVM-S4, CVM-S4.26, CVM-H and CVM-H+GTL.

Initial Test Case: 2008 Chino Hills Earthquake (I: 14383980)

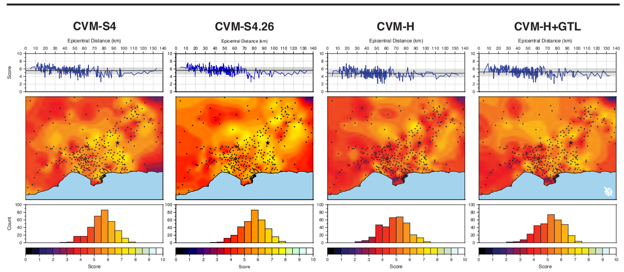

We used the 2008 Chino Hills earthquake as our initial test case. Simulation and validation results for this event had already been done for CVM-S4, CVM-H and CVM-H+GTL (Taborda and Bielak, 2013 & 2014 BSSA). We completed the set with a simulation using CVM-S4.26. Goodness-of-fit scores correspond to a modified version of Anderson's method (2004, WCEE), as indicated in Taborda and Bielak (2013, BSSA)

Validation Results

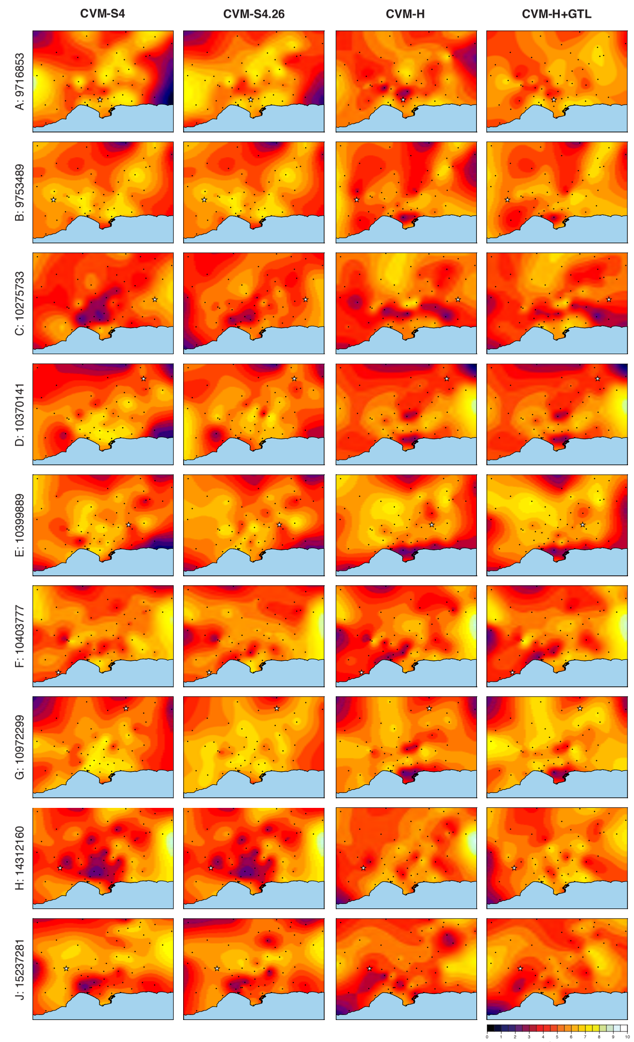

Goodness-of-fit contour maps have been computed for all the selected events. In the next phase of the project we will further process these results to try identify patters in the accuracy of the simulations that can be correlated to features particular to each velocity model.

Evaluation of the SCEC Seismic Velocity Models through Simulation and Validation of Past Earthquakes

Shima Azizzadeh-Roodpish,[1] Ricardo Taborda,[1,2] Naeem Khoshnevis,[1] Keli Cheng,[3]

1 Department of Civil Engineering, The University of Memphis
2 Center for Earthquake Research and Information, The University of Memphis
3 Lausanne Collegiate School, The University of Memphis

ASEIS Analysis and Simulation of Earthquake Impacts, Center for Earthquake Research and Information, The University of Memphis — USGS science for a changing world — SCEC an NSF+USGS center

Abstract

SCEC scientists have devoted significant effort over the last two decades to the development of various seismic velocity models for southern California. These models are mostly used in forward wave propagation simulation, but also as reference for tomographic and source inversions, and in other seismology and engineering problems. Two of these models, CVM-S and CVM-H, are among the most commonly used. This includes alternative variations such as the recently released model CVM-S4.26, which incorporates results from a sequence of tomographic inversions, and the user-controlled option of CVM-H to replace the near-surface profiles with a Vs30-based geotechnical layers (GTL) model. All four alternatives are thought acceptable, yet they have distinctions that lead to different results in forward simulations. The present study evaluates the accuracy of these models to predict the ground motion in the greater Los Angeles region through the validation of a series of past earthquake simulations. We present results for simulations of 30 moderate-magnitude earthquakes (3.5 < Mw < 5.5), and compare synthetics with data using a goodness-of-fit (GOF) method. The simulations are done with a finite element parallel code, with numerical models that satisfy a maximum frequency of 1 Hz and a minimum shear wave velocity of 200 m/s. We analyze the regional distribution of the GOF results for all events and all models, and search for correlations between the results and the characteristics of the models. Based on our comparisons, we identify which model consistently yields better results and present arguments that help explain why this is the case.

Study Area and Considered Earthquakes

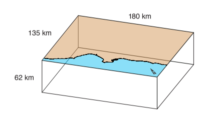

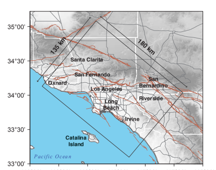

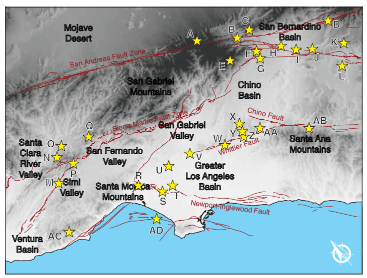

A set of 30 earthquakes between year 1998 to 2014 and magnitude of 3.6 to 5.4 and with depth between 3.6 and 21.1 km is modelled using a point source in the simulation domain, which covers all major basins in the greater Los Angeles region.

Code	Earthquake name	Event ID	Mw	Coordinates (lon., lat.)	Depth (m)	Strike/Dip/Rake	Date (yyy/mm/dd)	UTC Time (hh:mm:ss)
A	Wrightwood	9064568	4.40	-117.6480, 34.3740	8.99	285/57/86	1998/08/20	23:49:58.198
B	NW of Devore	10972299	3.79	-117.4642, 34.2655	10.91	98/58/68	2001/07/19	20:42:36.470
C	NNE of Devore	14494128	3.72	-117.3838, 34.2587	7.18	344/69/-33	2009/08/01	12:55:55.317
D	Yucaipa	14155260	4.88	-117.0113, 34.0580	11.61	75/59/55	2005/06/16	20:53:26.225
E	N of Rancho Cucamonga	10216101	3.60	-117.5762, 34.2058	4.92	54/69/16	2006/11/04	19:43:44.376
F	2002 Fontana	13692644	3.74	-117.4288, 34.1613	6.54	233/72/-28	2002/07/25	00:43:14.872
G	2005 Fontana	14116972	4.42	-117.4387, 34.1250	4.15	222/88/-25	2005/01/06	14:35:27.593
H	San Bernardino	10370141	4.45	-117.3042, 34.1073	14.22	87/70/28	2009/01/09	03:49:46.051
I	N of Loma Linda	9140050	4.37	-117.2525, 34.0500	15.36	270/90/-6	2000/02/21	13:49:43.017
J	Redlands	10541957	4.10	-117.1797, 34.0045	8.53	33/46/-68	2010/02/13	21:39:06.349
K	2010 Beaumont	10530013	4.28	-117.0232, 33.9322	13.93	234/89/9	2010/01/16	12:03:25.345
L	2006 Beaumont	14239184	3.90	-117.1122, 33.8560	11.53	45/31/-25	2006/07/10	02:54:43.809
M	Simi Valley	14000376	3.59	-118.7530, 34.2722	13.81	234/62/60	2003/10/29	23:44:48.206
N	WSW of Valencia	9753489	3.90	-118.6678, 34.3705	14.21	83/62/57	2002/01/29	06:00:39.140
O	Chatsworth	9096972	3.98	-118.6090, 34.3980	11.53	287/55/54	1999/07/22	09:57:23.502
P	Newhall	14312160	4.66	-118.6195, 34.2995	7.58	82/27/51	2007/08/09	07:58:48.888
Q	Beverly Hills	15237281	3.86	-118.4580, 34.3508	3.59	236/58/33	2012/10/28	15:24:23.172
R	Inglewood Area	9703873	4.24	-118.3885, 34.0590	7.90	262/81/4	2001/09/09	23:59:17.695
S	NW of Compton	10410337	4.70	-118.3357, 33.9377	13.86	243/60/25	2009/05/18	03:39:36.126
T	Downtown Los Angeles	9716853	3.98	-118.2702, 33.9290	31.13	116/68/71	2001/10/28	16:27:45.388
U	Whittier Narrows	9093975	3.77	-118.2180, 34.0100	9.53	125/49/79	1999/06/29	12:55:00.371
V	La Habra	14601172	4.44	-118.0817, 33.9923	18.85	282/36/73	2010/03/16	11:04:00.026
W	Chino Hills	15481673	5.10	-117.9300, 33.9200	5.00	239/70/38	2014/03/29	04:09:42.970
X	2002 Yorba Linda	14383980	5.39	-117.7613, 33.9530	14.70	47/51/32	2008/07/29	18:42:15.960
Y	2009 Yorba Linda	9818433	4.75	-117.7758, 33.9173	12.92	34/84/-10	2002/09/03	07:08:51.675
Z	2009 Yorba Linda	10399889	3.98	-117.7892, 33.8940	4.23	208/65/26	2009/04/24	03:27:49.840
AA	ESE of Yorba Linda	9644101	3.64	-117.6882, 33.8777	3.59	56/65/37	2001/04/13	11:50:11.916
AB	Lake Elsinore	10275733	4.73	-117.4770, 33.7322	12.60	65/59/58	2007/09/02	17:26:14.827
AC	Westlake Village	10403777	4.42	-118.8825, 34.0667	14.17	254/73/30	2009/05/02	01:11:13.084
AD	Hermosa Beach	14738436	3.69	-118.4578, 33.8572	11.23	57/41/54	2010/06/07	23:59:27.165

Methodology

The three steps of the projects are: Building velocity model for the region of southern California, Performing simulation for selected events using Hercules, a highly scalable end-to-end ground motion simulation engine part of the SCEC High-F platform, and processing and analyzing the results to identify possible patterns that can lead to recommendations on how to improve models and simulations.

Velocity Models and Simulation Results

The simulations of the selected events are all done for the four major velocity models currently available for the region of southern California: CVM-S4, CVM-S4.26, CVM-H and CVM-H+GTL.

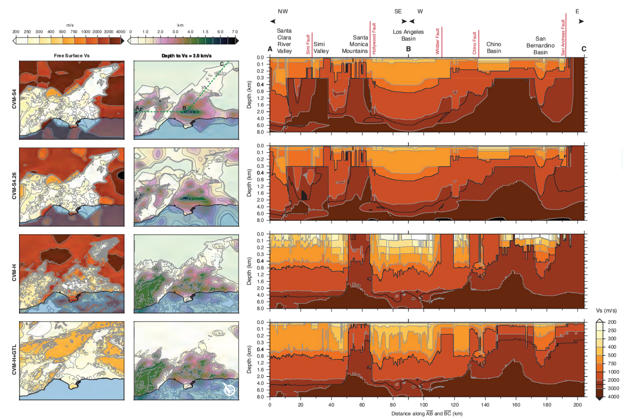

Plot of free surface Vs and the depths to the isosurface at which Vs value reach 2.5 km/s are presented for four models. Models have general similarities, specially between same families, but the differences can be seen as well. The strongest contrast is in the San Fernando, Santa Clara river and Simi valleys and the Ventura basin. Here the structure in CVM-H is deeper and wider than in CVMS. CVM-S4.26 exhibits deeper structures than CVM-S4.
We also compared two contiguous vertical profiles (Vs) along the segments AB and BC .

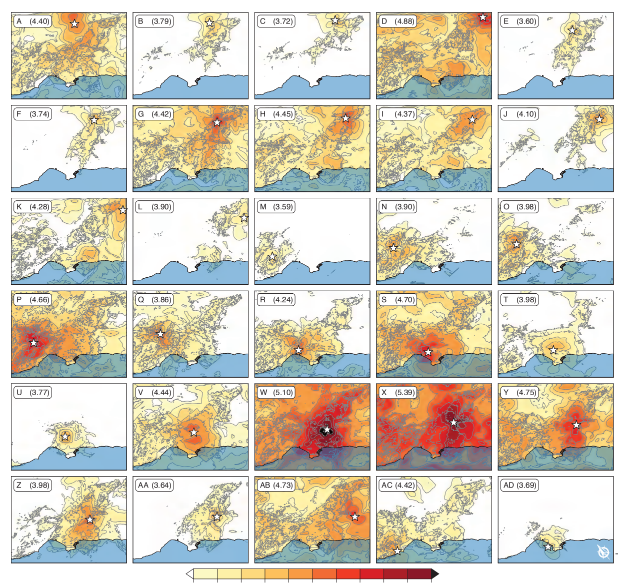

Free surface peak horizontal magnitude velocity from simulations for all the events using the velocity model CVM-S.26 are presented here.

Validation Results

Here simulation and validation results for three sample events are presented. Goodness-of-fit scores calculated for for CVM-S4.26, CVM-S4, CVM-H and CVM-H+GTL using a modified version of Anderson's method (2004, WCEE), as indicated in Taborda and Bielak (2013, BSSA).

2014 Mw 5.10 La Habra earthquake (W)

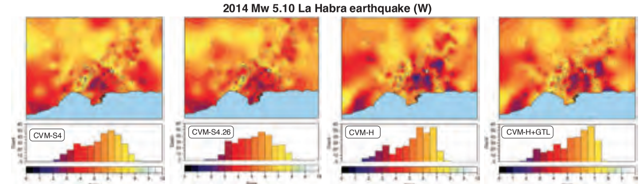

2008 Mw 5.39 Chino Hills Earthquake (X)

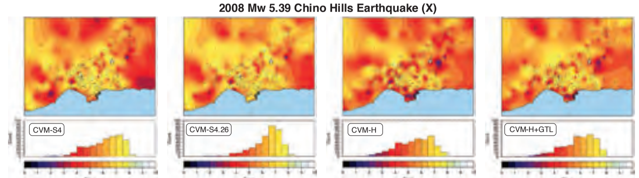

2001 Mw 3.79 near Devora, earthquake (B)

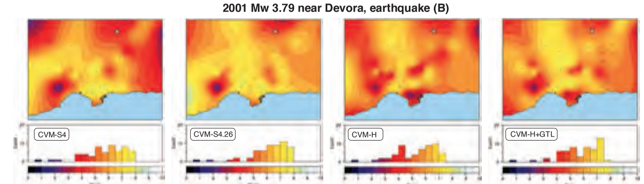

2009 Mw4.7 Inglewood Area earthquake (S)

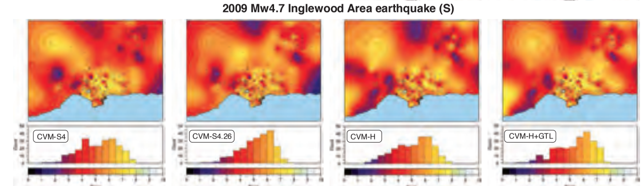

Goodness-of-fit have been computed for all the selected events and the results of the comparision are presented in the following graphs. The patterns to the accuracy of the simulations shows that the CVMS-4.26 model consistently yields better results. This indicates that previous observations made by taborda & Bielak (2014) and Lee et al (2014a) where not exclusive to limited events and the improvements done to CVM-S based on the tomographic studies done by Chen et al. (2007) and Lee et al. (2014a) have positive effects at frequencies above the limit considered for the inversions.